

Diagnosis and misdiagnosis of adult neuronal ceroid lipofuscinosis (Kufs disease)



Samuel F. Berkovic, MD,
FRS
John F. Staropoli, MD,
PhD
Stirling Carpenter, MD
Karen L. Oliver, MSc
Stanislav Kmoch, PhD
Glenn W. Anderson, MSc
John A. Damiano, BSc
Michael S. Hildebrand,
PhD
Katherine B. Sims, MD
Susan L. Cotman, PhD
Melanie Bahlo, PhD
Katherine R. Smith, PhD
Maxime Cadieux-Dion,
BSc
Patrick Cossette, MD,
PhD
Ivana Jedličková, MSc
Anna Přistoupilová, MSc
Sara E. Mole, PhD
On behalf of the ANCL
Gene Discovery
Consortium

Correspondence to
Dr. Berkovic:
s.berkovic@unimelb.edu.au

Supplemental data
at Neurology.org

ABSTRACT

Objective: To critically re-evaluate cases diagnosed as adult neuronal ceroid lipofuscinosis (ANCL) in order to aid clinicopathologic diagnosis as a route to further gene discovery.

Methods: Through establishment of an international consortium we pooled 47 unsolved cases regarded by referring centers as ANCL. Clinical and neuropathologic experts within the Consortium established diagnostic criteria for ANCL based on the literature to assess each case. A panel of 3 neuropathologists independently reviewed source pathologic data. Cases were given a final clinicopathologic classification of definite ANCL, probable ANCL, possible ANCL, or not ANCL.

Results: Of the 47 cases, only 16 fulfilled the Consortium's criteria of ANCL (5 definite, 2 probable, 9 possible). Definitive alternate diagnoses were made in 10, including Huntington disease, early-onset Alzheimer disease, Niemann-Pick disease, neuroserpinopathy, prion disease, and neurodegeneration with brain iron accumulation. Six cases had features suggesting an alternate diagnosis, but no specific condition was identified; in 15, the data were inadequate for classification. Misinterpretation of normal lipofuscin as abnormal storage material was the commonest cause of misdiagnosis.

Conclusions: Diagnosis of ANCL remains challenging; expert pathologic analysis and recent molecular genetic advances revealed misdiagnoses in >1/3 of cases. We now have a refined group of cases that will facilitate identification of new causative genes. [Neurology® 2016;87:579-584](https://doi.org/10.1212/WNL.0000000000002584)

GLOSSARY

ANCL = adult-onset neuronal ceroid lipofuscinosis; **CGP** = custom gene panel; **NCL** = neuronal ceroid lipofuscinosis; **WES** = whole-exome sequencing.

Diagnosis of neurodegenerative diseases in younger adults is challenging due to the relative rarity of the problem, the heterogeneous causes, and the frequent absence of noninvasive diagnostic clues, raising the question of brain biopsy. The neuronal ceroid lipofuscinoses (NCLs) are a group of storage diseases presenting from infancy to adulthood.¹ The stored material is largely made up of subunit c of mitochondrial adenosine triphosphate synthase or saposin proteins A and D—that is, of proteins so hydrophobic that they require special mechanisms for their breakdown and disposal.²

Adult-onset NCL (ANCL) is a particularly demanding diagnostic problem. Childhood NCLs have well-characterized clinical patterns typically involving brain and eye, abundant storage in readily accessible peripheral tissues such as skin, and largely solved molecular genetic causes.³⁻⁵ In contrast, ANCL can present in a variety of ways with progressive myoclonus epilepsy, dementia, or motor disorders and shows limited storage in peripheral tissue. Stored material is usually only found in a subset of neurons, with the accumulation of age-related lipofuscin

From the Epilepsy Research Centre, Department of Medicine (S.F.B., K.L.O., J.A.D., M.S.H.), University of Melbourne, Austin Health, Heidelberg, Australia; Biogen, Inc. (J.F.S.), Cambridge, MA; Department of Pathology (S.C.), Centro Hospitalar São João, Porto, Portugal; Institute of Inherited Metabolic Disorders (S.K., I.J., A.P.), First Faculty of Medicine, Charles University in Prague; General University Hospital in Prague (S.K.), Czech Republic; Great Ormond Street Hospital for Children NHS Foundation Trust (G.W.A.), London, UK; Center for Human Genetic Research and Department of Neurology (K.B.S., S.L.C.), Harvard Medical School, Massachusetts General Hospital, Boston; Population Health and Immunity Division (M.B., K.R.S.), The Walter and Eliza Hall Institute of Medical Research; Departments of Mathematics and Statistics and Medical Biology (M.B.), University of Melbourne, Australia; Centre de Recherche du Centre Hospitalier de l'Université de Montréal (M.C.-D., P.C.), University of Montreal, Canada; and MRC Laboratory for Cell Biology (S.E.M.), Department of Genetics, Evolution & Environment and UCL Institute of Child Health, University College London, UK.

Coinvestigators are listed on the [Neurology®](http://Neurology.org) Web site at Neurology.org.

Go to Neurology.org for full disclosures. Funding information and disclosures deemed relevant by the authors, if any, are provided at the end of the article.

often confused with pathologic storage.^{6–13} Furthermore, molecular genetic characterization of ANCL is at an early stage. Hindered by the small number of cases, and the clinical and pathologic challenges, ANCL is poorly understood.

Kufs disease is the best-known form of ANCL; it differs from most childhood-onset forms because there is no retinal involvement, and the inheritance can be either recessive or dominant. It is widely accepted that the uncommon teenage-onset cases without retinal involvement are grouped with adult-onset cases. The clinical presentation is variable with 2 broad forms identified. Kufs type A presents with progressive myoclonus epilepsy, whereas Kufs type B presents with dementia and motor signs.^{6,13} Recessive mutations in *CLN6*^{14–16} and dominant mutations in *DNAJC5*^{17–19} can cause Kufs type A; Kufs type B can be caused by recessive mutations in *CTSF*.^{20,21} Rare cases of ANCL with retinal involvement are described due to mutations in *PPT1 (CLN1)*,^{22,23} *CLN5*,^{24,25} and *GRN*.²⁶ Finally, some patients

with *CLN3* mutations present with neurologic manifestations in adult life, on a background of visual failure in childhood.²⁷

Despite these important molecular discoveries, many reported cases that receive a diagnosis of ANCL remain unsolved. As ANCL is rare, we formed a consortium to combine putative unsolved cases from centers around the world and analyzed them as one large cohort. We aimed to refine the clinical spectrum of late-onset NCL by implementing an expert clinical and pathologic review process, followed by consensus diagnosis. Here we report our somewhat surprising results, in particular, the frequent misdiagnosis of a broad spectrum of neurologic disorders as Kufs disease. Our eventual aim is to discover the remaining molecular causes of ANCL.

METHODS Participants. We established the ANCL Gene Discovery Consortium encompassing researchers with clinical, neuropathologic, and molecular genetic expertise in ANCL from the United Kingdom, Europe, United States, Canada, and Australia.

Consortium members pooled 47 unrelated, unsolved cases into a shared database. These cases had been referred to individual Consortium researchers for molecular genetic studies over a 20-year period because of diagnosis or putative diagnosis of ANCL. Clinicopathologic support for an ANCL diagnosis varied considerably in these cases that remained unsolved despite study by a variety of molecular genetic and enzymatic assays over time. For familial cases, only the proband was included. No attempt was made to sequence all known NCL genes before entry into the study.

Standard protocol approvals, registrations, and patient consents. Local institutional review boards at each contributing site approved this research. Participants or their guardians provided informed consent.

Diagnostic criteria. We developed initial diagnostic criteria based on a combination of clinical and pathologic features. These criteria were based on review of the literature and the clinical experience of Consortium members.^{6–13}

Clinical and pathologic review of cases. Strenuous attempts were made to source detailed clinical data from treating clinicians. We deliberately used broad clinical criteria (table 1) that allowed for retinal involvement.

Neuropathologic diagnosis remains the gold standard for this group of disorders. A panel of 3 expert neuropathologists (J.F.S., S.C., G.W.A.) developed criteria to classify the pathologic data as definite, probable, or possible NCL (table 1). Images of the pathologic material, where available, were subsequently shared with each of the 3 neuropathologists. They provided independent opinions, which were then discussed, and a consensus on the classification reached.

Overall classification of cases. Each case was given a final classification of definite ANCL, probable ANCL, possible ANCL, or not ANCL based on clinical and pathologic data. This occurred via regular Consortium teleconferences where the clinical criteria and pathologic classification were integrated to determine an overall classification (table 2).

Table 1 Adult-onset neuronal ceroid lipofuscinosis: Clinical and pathologic criteria

Clinical criteria (all 4 criteria required)
Age at onset between 12 and 60 years
Normal development and cognition prior to disease onset
Presence of at least 2 of the following: Seizures or myoclonus Progressive cognitive decline Ataxia Pyramidal or extrapyramidal motor signs
Documented deterioration over more than 2 years
Pathologic criteria
Definite pathologic features
Ultrastructural demonstration of one or more characteristic membrane-bound storage morphologies (granular osmiophilic deposits [GRODs], fingerprint profiles, curvilinear profiles, or rectilinear complexes) in more than one cell type, including but not limited to eccrine secretory and duct cells, endothelial cells, smooth and skeletal muscle cells, or neurons or their proximal axons. Fingerprint profiles in vascular smooth muscle and pericytes are excluded, since it has been shown that they accumulate there nonspecifically with aging ³⁵
Probable pathologic features
Ultrastructural demonstration of one or more characteristic membrane-bound storage morphologies (GRODs, fingerprint profiles, curvilinear profiles, or rectilinear complexes) in a single cell type AND Demonstration, in standard histologic preparations, of cytoplasmic inclusions with broad-range autofluorescence or Luxol fast blue positivity in well-differentiated sections in one or more of above cell types, to a degree significantly greater than expected for age, OR Demonstration, by standard immunohistochemistry, of characteristic cytoplasmic storage material, i.e., subunit c of mitochondrial adenosine triphosphate synthase, saposin protein A, or saposin protein D
Possible pathologic features (in absence of ultrastructural data)
Demonstration, in standard histologic preparations, of cytoplasmic inclusions with broad-range autofluorescence or Luxol fast blue positivity in well-differentiated sections in one or more of the above cell types, to a degree significantly greater than expected for age

Table 2 Adult-onset neuronal ceroid lipofuscinosis (ANCL) classification criteria incorporating both clinical and pathologic criteria (see table 1) for 47 putative cases

ANCL classification	Clinicopathologic criteria	No. of cases
Definite ANCL	All clinical criteria met plus definite pathology classification	5 ^a
Probable ANCL	Atypical clinical presentation (e.g., late onset) plus definite pathology classification All clinical criteria met plus probable pathology classification	2
Possible ANCL	Atypical clinical presentation plus probable pathology classification All clinical criteria met plus possible pathology classification	9
Not ANCL	Clinical, pathologic, or molecular data strongly suggesting an alternate diagnosis Review of images or source material suggests no evidence of neuronal ceroid lipofuscinosis Pathology images unavailable (i.e., report only)	31

^aOne case had a compound heterozygous *CLN6* mutation.

Molecular genetic studies. Screening for known ANCL genes (*CLN6*, *CTSF*, *DNAJC5*, *GRN*, and *PPT1*) was performed by both Sanger sequencing and high-throughput sequencing technologies in the majority of the 16 cases (detailed in table

e-1 on the *Neurology*[®] Web site at Neurology.org). Genomic DNA was extracted from venous blood using standard methods. Briefly, for Sanger sequencing, coding exons and flanking intronic regions including splice sites of the 3 genes were PCR amplified using primers designed for all isoforms with reference human gene transcripts (NCBI Gene; <http://www.ncbi.nlm.nih.gov/>; primers available on request). Amplification reactions were cycled on a Veriti Thermal Cycler (Applied Biosystems, Carlsbad, CA) and bidirectional sequencing was completed using BigDye v3.1 Terminator Cycle Sequencing Kit (Applied Biosystems). Sequencing products were resolved using a 3730xl DNA Analyzer (Applied Biosystems). Sequence chromatograms were compared to published cDNA sequence with nucleotide changes detected using Codon Code Aligner (CodonCode Corporation, Dedham, MA).

A custom gene panel (CGP), designed to target coding regions (6.88 Mb) of 3,616 OMIM genes with known phenotypes including ANCL, and whole-exome sequencing (WES) was also performed for the majority (table e-1). DNA enrichment was performed according to the manufacturer's protocol using either SeqCap EZ Choice Library (Roche Nimblegen, Madison, WI) for the CGP or Nimblegen SeqCap V3 (Roche Nimblegen) for WES. DNA sequencing was performed on the captured barcoded DNA libraries using either SOLiD 4 System (Applied Biosystems) or

Table 3 Summary of 10 cases with an initial diagnosis of adult-onset neuronal ceroid lipofuscinosis (ANCL) in which an alternate diagnosis was later confirmed

Case	Clinical features	Initial ANCL diagnosis	Diagnostic reevaluation	Final diagnosis
KC23	Onset mid-20s with motor and intellectual deterioration (dementia); no seizures; progressive ataxia but no distinct chorea; autosomal dominant family history	Clinical history consistent with ANCL; skin biopsy interpreted as showing fingerprint profiles	Pathology review: normal lipofuscin; clinical review suggested Huntington disease; genetic diagnosis: <i>HTT</i> expansion	Huntington disease
KC33	Onset 28 years with cognitive decline; seizure history unknown; deceased in 40s	Clinical history consistent with ANCL; brain biopsy interpreted as showing autofluorescent inclusions and GROD-like material	Pathology review: Normal lipofuscin; genetic diagnosis: <i>NPC1</i> mutation	Niemann-Pick syndrome
KC51	Onset 34 years; dementia with frontal features, subtle facial dyskinesia, parkinsonian and mild cerebellar features including limb ataxia; no seizures; autosomal recessive family history	Clinical history consistent with ANCL; skin biopsy interpreted as showing fingerprint profiles in sweat glands	Pathology review: normal lipofuscin; genetic diagnosis: <i>PLA2G6</i> p.G551S mutation	Neurodegeneration with brain iron accumulation
KC35	Onset 20s with progressive cognitive decline followed by tremor, myoclonus, and ataxia	Clinical history consistent with ANCL; skin biopsy interpreted as showing membrane-bound inclusions with granular material	Pathology review: images of source material not available; genetic diagnosis: <i>c19orf12</i> mutation	Neurodegeneration with brain iron accumulation
KC10	Onset age 29 with rapidly progressing dementia, motor deterioration, and myoclonus	Clinical history consistent with ANCL; rectal biopsy identified electron-dense structure interpreted as fingerprints and curvilinear pattern consistent with NCL	Pathology review: images of source material not available; brain biopsy revealed malignant lymphocytes	Cerebral Lymphoma
KC24	Onset 22 years; myoclonus and tonic-clonic seizures; cognitive decline; personality change; unsteady gait from early 20s leading to wheelchair dependence; deceased at 26 years	Clinical history consistent with ANCL; postmortem brain biopsy interpreted as consistent with ceroid lipofuscinosis	Pathology review: extensive lesion of the thalamus consistent with "familial" fatal insomnia; immunohistochemistry: PrP ^{Sc} positive; genetic diagnosis: <i>PRNP</i> insertion c.154_177[6_13]	Prion disease
KC29	Onset at 13 years with myoclonus; tonic-clonic seizures and absences at 15 years; progressive ataxia; wheelchair-bound at 22 years; late ophthalmoplegia; mild learning disability	Clinical history consistent with ANCL; skin and muscle biopsy negative	Pathology review: images of source material not available; genetic diagnosis: hypothesis free whole exome sequencing showed <i>SACS</i> p.P2798Q; p.T458I mutation ³⁶	Autosomal recessive spastic ataxia of Charlevoix-Saguenay
KC8	Onset at 33 years with gait ataxia and subsequent dementia, dystonia, and psychiatric symptoms; no seizures; autosomal dominant family history	Clinical history consistent with ANCL; premortem biopsies not done	Autopsy revealed classical Alzheimer disease; genetic diagnosis: <i>PSEN1</i> p.S170F; <i>CTSD</i> p.A58V ³⁷	Early-onset familial Alzheimer disease
KC21	Onset at 13 years with behavioral changes (frontal dysfunction) and declining school performance; myoclonus with occasional tonic-clonic seizures and poor coordination	Clinical history consistent with ANCL; no pathology (biopsy not done)	Genetic diagnosis: hypothesis free whole exome sequencing showed <i>SERPINI1</i> p.G392E mutation ³⁶	Neuroserpinopathy
KC7	Onset age 19 years; progressive disease with myoclonus, epilepsy, and ataxia	Clinical history consistent with ANCL; skin, muscle, and brain biopsy negative	Pathology review: images of source material not available; genetic diagnosis: <i>MTND3</i> mutation	Leigh syndrome

Illumina HiSeq 1500. Data analysis was performed as previously described.²⁸ The data were inspected for variations in known ANCL genes and the search for novel genes is ongoing.

Molecular diagnosis of cases initially suspected of having ANCL, where other disorders were later established, were performed at a number of commercial and research laboratories using standard techniques.

RESULTS Of the 47 Consortium cases, 16 cases fulfilled the Consortium's clinical and pathologic criteria for definite, probable, or possible ANCL disease (table 2). Of the 16 cases, 8 (2 definite) presented with seizures as a main feature, usually with a progressive myoclonus epilepsy (Type A Kufs). The remaining 8 cases (3 definite) presented with dementia and motor signs (Type B Kufs). None of the ANCL cases had retinal involvement. The mean age at onset was 35 years (median 35.5 years). There were 2 clusters; 6 had onset in the second decade of life and 10 in the fourth decade or later. Both Type A and Type B cases were represented in the 2 age clusters. Two cases fell outside of our arbitrary 12- to 60-years range for disease onset (onset at 10 and 62 years); these cases were considered clinically atypical and classified overall as possible ANCL (table 2).

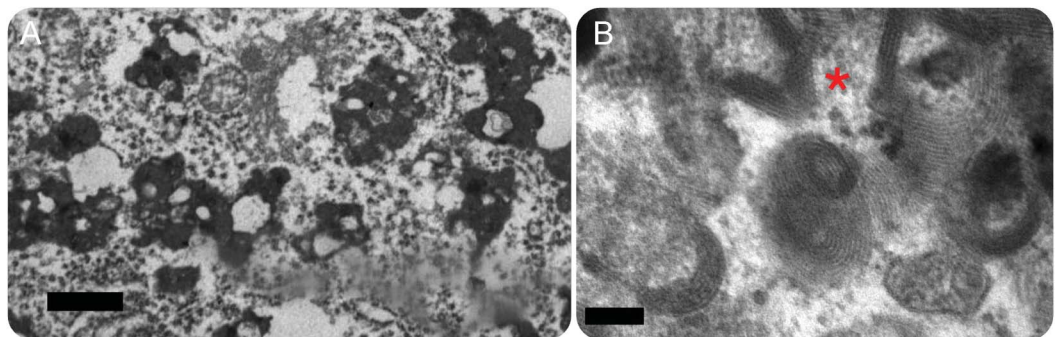
A family history suggestive of dominant inheritance was found in 4/16 ANCL cases; in 12, there was no family history. *DNAJC5* mutations were not found in the 4 dominant cases or the 10 other cases that had this gene sequenced. *CLN6* and *CTSF*, known causes of recessive ANCL, were sequenced in 15 cases and 1 case had probable pathogenic compound heterozygous *CLN6* variants identified. This patient was classified as definite ANCL with a Type A presentation. This leaves a subset of 15 genetically unsolved ANCL cases (4 definite).

Our criteria for ANCL were not met in 31/47 (66%) cases, including 2 cases previously published in detail as having ANCL.^{29,30} In 10 of these 31 cases, detailed review with further investigation established definitive alternate diagnoses (table 3). The main reason for misdiagnosis as ANCL was overinterpretation of normal age-related lipopigment as pathologic storage material (figure). Six cases had features suggesting that ANCL was not the correct diagnosis. Two of these had storage material without the characteristics of the lipopigment seen in NCL, but a specific diagnosis could not be made. Two had other neuropathologic abnormalities, again without leading to a specific diagnosis. In 2 cases, biopsy material reported as suggestive of NCL was considered nonspecific on review, and the clinical features were atypical. In the remaining 15 cases, the clinical and pathologic data were inadequate for classification.

DISCUSSION In this study of 47 cases considered to have ANCL, we found that the diagnosis could be supported in only 16 cases; of these, 9 were considered possible cases. Moreover, ANCL was confidently excluded in 16 cases, of which 10 had secure alternative diagnoses established. The classification criteria developed by the Consortium were useful in formalizing the approach to problematic cases and has highlighted the challenges and subtleties in diagnosing ANCL.

The pathologic diagnosis is challenging and is compounded by the relative rarity of these disorders such that most neuropathologists have very limited experience with the condition. In general, misdiagnosis occurred by overinterpretation of ultrastructural findings in biopsy samples, with failure to distinguish

Figure Pathologic diagnosis and misdiagnosis of adult-onset neuronal ceroid lipofuscinosis (ANCL)



(A) Electron micrograph of KC33 shows one of many deposits of lipofuscin in a cortical neuron. These deposits were originally considered to represent granular osmiophilic deposits (GRODs), leading to a diagnosis of ANCL. Lipid vacuoles, as seen here, are numerous in lipofuscin, but not in GRODs, and the granules in lipofuscin are coarser and less uniform (bar = 5 μ m). The patient had cognitive decline beginning at age 28 years; *NPC1* mutation was later found (table 3). (B) This electron micrograph of KC15 shows fingerprint profiles from an eccrine secretory cell. The basic paired parallel line pattern even at this magnification tends to appear as a single wide slightly fuzzy line, but the spacing, the wheeling ranks, and the focal crystalline pattern where the ranks intersect (at the left of the asterisk) are very characteristic (bar = 1 μ m). Disease onset was at 18 years with stimulus-sensitive and action-induced myoclonus, dementia, and parkinsonism on the background of normal development. This case met out criteria for classification as definite ANCL. The molecular basis remains unknown.

normal lipofuscin that accumulates with age, from abnormal lipopigment seen in NCL, which may be very limited in ANCL.^{6–13} In children, this distinction is easier, contrasting abundant storage in disease with minimal normal age-related pigment. Rather than relying on the amount of lipopigment, accurate diagnosis depends on analysis of the particular ultrastructural features.^{7,31} In all late-onset neuronal storage diseases, only a subset of neurons may be involved. This becomes important when it comes to electron microscopy on a brain biopsy. If the blocks have not been trimmed to include involved neurons, the study may be limited to normal neurons that inevitably contain lipofuscin, and confusion with ANCL may result.

Importantly, the removal of these cases from the cohort helps simplify the apparent clinical and pathologic heterogeneity of ANCL. The clinical profile of our ANCL cases fit broadly into the previously described categories of presentation as progressive myoclonus epilepsy (Type A) and dementia with motor disturbances (Type B)⁶; the single case that was solved molecularly with a *CLN6* mutation had a Type A presentation, as has been previously described.¹⁴

The degree of genetic heterogeneity of ANCL remains unclear. It is already known that contrary to the childhood forms, which are essentially all recessive disorders, the adult forms can have either recessive or dominant inheritance.^{6,32,33} While it is now possible to survey the whole exome (or genome) for genetic variation with high-throughput sequencing technology, determining which of the many thousand variants identified are pathogenic remains challenging. However, this is still a good option for treating clinicians and may avoid the need for brain biopsy should a plausible variant be found in one of the known ANCL genes or in a gene known to cause an alternative late-onset neurologic disease. The efficacy of genetic testing for diagnostic purposes will only improve as further ANCL genes are discovered. At this point in time, pathologic diagnosis remains the gold standard practice.

Future research into the underlying genetic etiology of the unsolved ANCL will be supported by the removal of misdiagnosed cases that would hinder these important efforts. By pooling together unrelated ANCL cases that putatively may share the same causative gene, the genomic search space can be considerably narrowed. This ongoing work, resulting in a deeper understanding of the molecular genetic basis, will provide improved guidance for the accurate and early diagnosis of ANCL. We anticipate that the recently accepted nomenclature for the NCL³⁴ will be expanded as new genes are identified.

AUTHOR CONTRIBUTIONS

Dr. Berkovic drafted/revised the manuscript for content, contributed to study concept/design, contributed to acquisition of the data, performed analysis/interpretation of the data, and provided study supervision and

coordination. Dr. Staropoli revised the manuscript for content, contributed to study concept/design, contributed to acquisition of the data, performed analysis/interpretation of the data, and provided study coordination. Dr. Carpenter revised the manuscript for content and performed analysis/interpretation of the data. K.L. Oliver drafted/revised the manuscript for content, contributed to acquisition of the data, performed analysis/interpretation of the data, and provided study coordination. Dr. Kmoch revised the manuscript for content, contributed to study concept/design, contributed to acquisition of the data, and performed analysis/interpretation of the data. G.W. Anderson revised the manuscript for content and performed analysis/interpretation of the data. J.A. Damiano revised the manuscript for content and performed analysis/interpretation of the data. Dr. Hildebrand revised the manuscript for content and performed analysis/interpretation of the data. Dr. Sims revised the manuscript for content, contributed to acquisition of the data, and performed analysis/interpretation of the data. Dr. Cotman revised the manuscript for content, contributed to acquisition of the data, and performed analysis/interpretation of the data. Dr. Bahlo revised the manuscript for content and performed analysis/interpretation of the data. Dr. Smith revised the manuscript for content and performed analysis/interpretation of the data. M. Cadieux-Dion revised the manuscript for content and performed analysis/interpretation of the data. Dr. Cossette revised the manuscript for content and contributed to acquisition of the data. I. Jedličková revised the manuscript for content and performed analysis/interpretation of the data. A. Přistoupilová revised the manuscript for content and performed analysis/interpretation of the data. Dr. Mole revised the manuscript for content, contributed to study concept/design, contributed to acquisition of the data, performed analysis/interpretation of the data, and provided study coordination.

STUDY FUNDING

S.F.B. was supported by a National Health and Medical Research Council Program Grant (ID: 628952). S.K., I.J., and A.P. are funded by Charles University institutional programs PRVOUK-P24/LF1/3, UNCE 204011, and SVV2016/260148 and by the project LQ1604 NPU II from the Ministry of Education of the Czech Republic. This work was specifically supported by grant 15-28208A from the Ministry of Health of the Czech Republic and GA UK No. 269615 (I.J.) and No. 1402213 (A.P.). Instrumental support for exome and gene panel sequencing was provided by the Genomic facility in Motol University Hospital in Prague (OPPK.CZ.2.16/3.100/24022). S.E.M. received specific funding towards the work of the Rare NCL Gene Consortium and Kufs disease from the USA Batten Disease Support and Research Association. S.L.C. is funded by the National Institutes of Health: National Institute of Neurologic Disorders & Stroke (R01NS073813). M.C.-D. is supported by the Fonds de Recherche du Québec–Santé (FRQS).

DISCLOSURE

S. Berkovic has served on scientific advisory boards for UCB and Janssen-Cilag; serves on the editorial boards of *Lancet Neurology* and *Epileptic Disorders* and the Advisory Board of *Brain*; may accrue future revenue on pending patent WO61/010176: Therapeutic Compound that relates to discovery of PCDH19 gene as the cause of familial epilepsy with mental retardation limited to females; is one of the inventors listed on a patent held by Bionomics Inc. on diagnostic testing using the *SCN1A* gene, WO2006/133508; has received speaker honoraria from UCB; has received unrestricted educational grants from UCB, Janssen-Cilag, and Sanofi-Aventis; and receives/has received research support from the National Health and Medical Research Council of Australia and NINDS. J. Staropoli, S. Carpenter, K. Oliver, S. Kmoch, G. Anderson, J. Damiano, M. Hildebrand, K. Sims, S. Cotman, M. Bahlo, K. Smith, M. Cadieux-Dion, P. Cossette, I. Jedličková, A. Přistoupilová, and S. Mole report no disclosures relevant to the manuscript. Go to Neurology.org for full disclosures.

Received November 15, 2015. Accepted in final form April 29, 2016.

REFERENCES

1. Mole SE, Williams RE, Goebel HH. The Neuronal Ceroid Lipofuscinoses (Batten Disease). 2nd ed. Oxford: Oxford University Press; 2011.

2. Palmer DN, Barry LA, Tyynela J, Cooper JD. NCL disease mechanisms. *Biochim Biophys Acta* 2013;1832:1882–1893.
3. Kousi M, Lehesjoki AE, Mole SE. Update of the mutation spectrum and clinical correlations of over 360 mutations in eight genes that underlie the neuronal ceroid lipofuscinoses. *Hum Mutat* 2012;33:42–63.
4. Mole SE. NCL Mutation and Patient Database [online]. Available at: <http://www.ucl.ac.uk/ncl/mutation.shtml>. Accessed November 1, 2015.
5. Kmoch S, Stranecky V, Emes RD, Mitchison HM. Bioinformatic perspectives in the neuronal ceroid lipofuscinoses. *Biochim Biophys Acta* 2013;1832:1831–1841.
6. Berkovic SF, Carpenter S, Andermann F, et al. Kufs' disease: a critical reappraisal. *Brain* 1988;111:27–62.
7. Anderson G, Elleder M, Goebel HH. Morphological diagnostic and pathological considerations. In: Mole SE, Williams RE, Goebel HH, eds. *The Neuronal Ceroid Lipofuscinoses (Batten Disease)*. 2nd ed. Oxford: Oxford University Press; 2011:35–49.
8. Anderson GW, Goebel HH, Simonati A. Human pathology in NCL. *Biochim Biophys Acta* 2013;1832:1807–1826.
9. Carpenter S. Morphological diagnosis and misdiagnosis in Batten-Kufs disease. *Am J Med Genet Suppl* 1988;5:85–91.
10. Goebel HH, Braak H. Adult neuronal ceroid-lipofuscinosis. *Clin Neuropathol* 1989;8:109–119.
11. Goebel HH, Sharp JD. The neuronal ceroid-lipofuscinoses: recent advances. *Brain Pathol* 1998;8:151–162.
12. Pasquinelli G, Cenacchi G, Piane EL, et al. The problematic issue of Kufs disease diagnosis as performed on rectal biopsies: a case report. *Ultrastruct Pathol* 2004;28:43–48.
13. Sadzot B, Reznik M, Arrese-Estrada JE, Franck G. Familial Kufs' disease presenting as a progressive myoclonic epilepsy. *J Neurol* 2000;247:447–454.
14. Arsov T, Smith KR, Damiano J, et al. Kufs disease, the major adult form of neuronal ceroid lipofuscinosis, caused by mutations in *CLN6*. *Am J Hum Genet* 2011;88:566–573.
15. Andrade DM, Paton T, Turnbull J, et al. Mutation of the *CLN6* gene in teenage-onset progressive myoclonus epilepsy. *Pediatr Neurol* 2012;47:205–208.
16. Canafoglia L, Gilioli I, Invernizzi F, et al. Electroclinical spectrum of the neuronal ceroid lipofuscinoses associated with *CLN6* mutations. *Neurology* 2015;85:316–324.
17. Cadieux-Dion M, Andermann E, Lachance-Touchette P, et al. Recurrent mutations in *DNAJC5* cause autosomal dominant Kufs disease. *Clin Genet* 2013;83:571–575.
18. Noskova L, Stranecky V, Hartmannova H, et al. Mutations in *DNAJC5*, encoding cysteine-string protein alpha, cause autosomal-dominant adult-onset neuronal ceroid lipofuscinosis. *Am J Hum Genet* 2011;89:241–252.
19. Velinov M, Dolzhanskaya N, Gonzalez M, et al. Mutations in the gene *DNAJC5* cause autosomal dominant Kufs disease in a proportion of cases: study of the Parry family and 8 other families. *PLoS One* 2012;7:e29729.
20. Smith KR, Dahl HH, Canafoglia L, et al. Cathepsin F mutations cause type B Kufs disease, an adult-onset neuronal ceroid lipofuscinosis. *Hum Mol Genet* 2013;22:1417–1423.
21. Di Fabio R, Moro F, Pestillo L, et al. Pseudo-dominant inheritance of a novel *CTSF* mutation associated with type B Kufs disease. *Neurology* 2014;83:1769–1770.
22. van Diggelen OP, Thobois S, Tilikete C, et al. Adult neuronal ceroid lipofuscinosis with palmitoyl-protein thioesterase deficiency: first adult-onset patients of a childhood disease. *Ann Neurol* 2001;50:269–272.
23. Ramadan H, Al-Din AS, Ismail A, et al. Adult neuronal ceroid lipofuscinosis caused by deficiency in palmitoyl protein thioesterase 1. *Neurology* 2007;68:387–388.
24. Sleat DE, Ding L, Wang S, et al. Mass spectrometry-based protein profiling to determine the cause of lysosomal storage diseases of unknown etiology. *Mol Cell Proteomics* 2009;8:1708–1718.
25. Xin W, Mullen TE, Kiely R, et al. *CLN5* mutations are frequent in juvenile and late-onset non-Finnish patients with NCL. *Neurology* 2010;74:565–571.
26. Smith KR, Damiano J, Franceschetti S, et al. Strikingly different clinicopathological phenotypes determined by progranulin-mutation dosage. *Am J Hum Genet* 2012;90:1102–1107.
27. Lauronen L, Munroe PB, Jarvela I, et al. Delayed classic and protracted phenotypes of compound heterozygous juvenile neuronal ceroid lipofuscinosis. *Neurology* 1999;52:360–365.
28. Park EJ, Grabinska KA, Guan Z, et al. Mutation of Nogo-B receptor, a subunit of cis-prenyltransferase, causes a congenital disorder of glycosylation. *Cell Metab* 2014;20:448–457.
29. Reif A, Schneider MF, Hoyer A, et al. Neuroleptic malignant syndrome in Kufs' disease. *J Neurol Neurosurg Psychiatry* 2003;74:385–387.
30. Zini A, Cenacchi G, Nichelli P, et al. Early-onset dementia with prolonged occipital seizures: an atypical case of Kufs disease. *Neurology* 2008;71:1709–1712.
31. Carpenter S, Karpati G, Andermann F, et al. The ultrastructural characteristics of the abnormal cytosomes in Batten-Kufs' disease. *Brain* 1977;100:137–156.
32. Boehme DH, Cottrell JC, Leonberg SC, Zeman W. A dominant form of neuronal ceroid-lipofuscinosis. *Brain* 1971;94:745–760.
33. Burneo JG, Arnold T, Palmer CA, Kuzniecky RI, Oh SJ, Faught E. Adult-onset neuronal ceroid lipofuscinosis (Kufs disease) with autosomal dominant inheritance in Alabama. *Epilepsia* 2003;44:841–846.
34. Williams RE, Mole SE. New nomenclature and classification scheme for the neuronal ceroid lipofuscinoses. *Neurology* 2012;79:183–191.
35. Ferlazzo E, Gasparini S, Pasquinelli G, et al. Usefulness of rectal biopsy for the diagnosis of Kufs disease: a controlled study and review of the literature. *Eur J Neurol* 2012;19:1331–1336.
36. Muona M, Berkovic SF, Dibbens LM, et al. A recurrent de novo mutation in *KCNC1* causes progressive myoclonus epilepsy. *Nat Genet* 2015;47:39–46.
37. Ehling R, Nosková L, Stranecký V, et al. Cerebellar dysfunction in a family harboring the PSEN1 mutation cosegregating with a cathepsin D variant p.A58V. *J Neurol Sci* 2013;326:75–82.

Teenage-onset progressive myoclonic epilepsy due to a familial *C9orf72* repeat expansion

Jelle van den Aemele, MD, PhD,* Ivana Jedlickova, MSc,* Anna Pristoupilova, MSc, Anne Sieben, MD, Sara Van Mossevelde, MD, Chantal Ceuterick-de Groote, PhD, Helena Hůlková, MD, PhD, Radoslav Matej, MD, PhD, Alfred Meurs, MD, PhD, Christine Van Broeckhoven, PhD, DSc, Samuel F. Berkovic, MD, Patrick Santens, MD, PhD, Stanislav Kmoč, PhD, and Bart Dermaut, MD, PhD

Neurology® 2018;90:1-6. doi:10.1212/WNL.0000000000004999

Correspondence

Dr. van den Aemele
jv361@cam.ac.uk or
Dr. Dermaut
bart.dermaut@ugent.be

Abstract

Background

The progressive myoclonic epilepsies (PME) are a heterogeneous group of disorders in which a specific diagnosis cannot be made in a subset of patients, despite exhaustive investigation. *C9orf72* repeat expansions are emerging as an important causal factor in several adult-onset neurodegenerative disorders, in particular frontotemporal lobar degeneration and amyotrophic lateral sclerosis. An association with PME has not been reported previously.

Objective

To identify the causative mutation in a Belgian family where the proband had genetically unexplained PME.

Results

We report a 33-year old woman who had epilepsy since the age of 15 and then developed progressive cognitive deterioration and multifocal myoclonus at the age of 18. The family history suggested autosomal dominant inheritance of psychiatric disorders, epilepsy, and dementia. Thorough workup for PME including whole exome sequencing did not reveal an underlying cause, but a *C9orf72* repeat expansion was found in our patient and affected relatives. Brain biopsy confirmed the presence of characteristic p62-positive neuronal cytoplasmic inclusions.

Conclusion

C9orf72 mutation analysis should be considered in patients with PME and psychiatric disorders or dementia, even when the onset is in late childhood or adolescence.

*These authors contributed equally to this work.

From the Department of Neurology (J.v.d.A., A.S., A.M., P.S., B.D.) and Center for Medical Genetics (B.D.), Ghent University Hospital, Belgium; Institute for Inherited Metabolic Disorders (I.J., A.P., H.H., S.K.), Prague, First Faculty of Medicine, Charles University in Prague, Czech Republic; Neurodegenerative Brain Diseases Group (A.S., S.V.M., C.V.B.), Center for Molecular Neurology, VIB; Neuropathology and Laboratory of Neurochemistry and Behavior (A.S.), Laboratory of Neurogenetics (S.V.M., C.V.B.), and Laboratory of Neuro-muscular Pathology and Translational Neurosciences (C.C.-d.G.), Institute Born-Bunge, University of Antwerp, Belgium; Institute of Pathology, First Faculty of Medicine (H.H., R.M.), Charles University and General University Hospital; Department of Pathology and Molecular Medicine (R.M.), National Reference Laboratory for Diagnostics of Human Prion Diseases, Thomayer Hospital, Prague, Czech Republic; Epilepsy Research Centre, Department of Medicine (S.F.B.), University of Melbourne, Austin Health, Heidelberg, Australia; and Inserm U1167 (B.D.), Laboratoire d'Excellence Distalz, Institut Pasteur de Lille, Longevity Research Center, Université de Lille, France. J.v.d.A. is currently affiliated with the Department of Clinical Neurosciences and WT/CRUK Gurdon Institute, University of Cambridge, UK.

Go to Neurology.org/N for full disclosures. Funding information and disclosures deemed relevant by the authors, if any, are provided at the end of the article.

Glossary

ALS = amyotrophic lateral sclerosis; **ANCL** = adult neuronal ceroid lipofuscinosis; **EM** = electron microscopy; **FTD** = frontotemporal dementia; **NCL** = neuronal ceroid lipofuscinoses; **PME** = progressive myoclonic epilepsies; **WES** = whole exome sequencing.

The progressive myoclonic epilepsies (PME) are a heterogeneous group of neurodegenerative diseases with variable age at onset and cause, all resulting in a progressive syndrome of myoclonic jerks and epileptic seizures, often accompanied by dementia and ataxia.¹ There are over 20 established genetic causes of PME with the more common ones being Unverricht-Lundborg and Lafora body disease due to mutations in *CSTB* and *EPM2A/EPM2B*, respectively, the neuronal ceroid lipofuscinoses (NCL), sialidoses due to neuraminidase deficiency, and mitochondrial encephalopathy with ragged red fibers. A recent large multicenter study could not identify an underlying cause in 28% of patients with PME.²

C9orf72 hexanucleotide repeat expansions are the main cause of genetic frontotemporal dementia (FTD) and amyotrophic lateral sclerosis (ALS). Average age at onset is in the 6th decade, with a range between 27 and 83 years.^{3,4} Since their first description in 2011,⁵⁻⁷ the clinical phenotype associated with these mutations has expanded beyond the FTD/ALS spectrum. Parkinsonism and psychiatric features are well established now, and hyperkinetic or cerebellar movement disorders have been described.^{8,9} Seizures are rarely described^{10,11} and PME has not been reported.

We describe a patient with PME and a *C9orf72* repeat expansion, with first symptoms appearing at the age of 15. Onset in the pediatric years and the phenotype of PME broadens the *C9orf72*-related phenotypic spectrum and could provide an opportunity for patients with PME for whom no underlying cause has been detected.

Case report

A 33-year-old woman was referred to the neurology department of a tertiary care hospital in Belgium because of progressive cognitive decline and speech difficulties. She had had epilepsy with generalized tonic-clonic seizures and myoclonic jerks since the age of 15 but was seizure-free for several years under treatment with valproic acid, levetiracetam, and clobazam. She was reportedly well before the age of 15, with average school performance. She lived with her partner and could perform all activities of daily life independently. Despite attempting higher education at the age of 18, she did not succeed and was currently employed in a sheltered workshop.

On clinical examination, the patient was alert and cooperative, and was well-oriented in time and space. She had

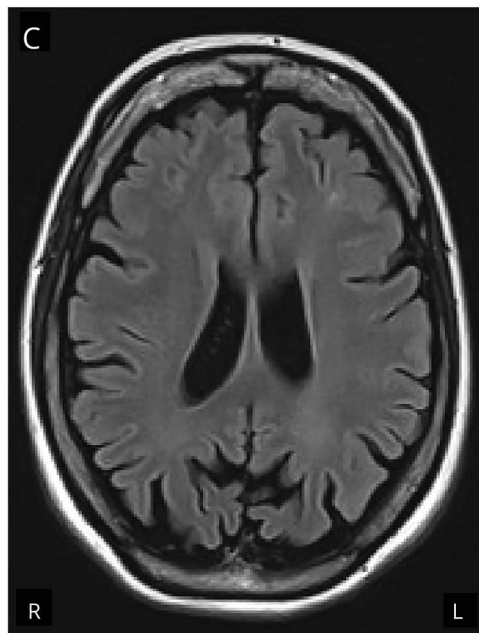
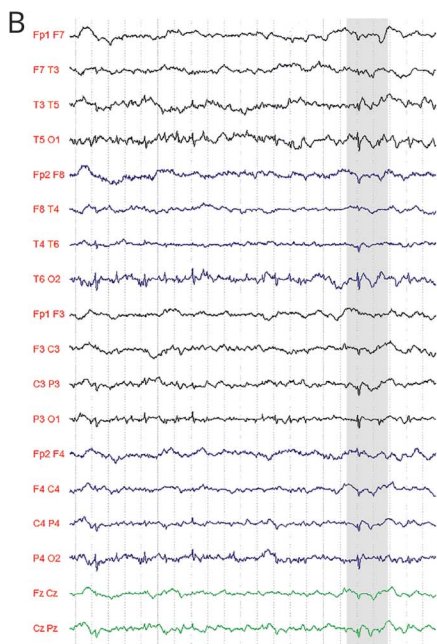
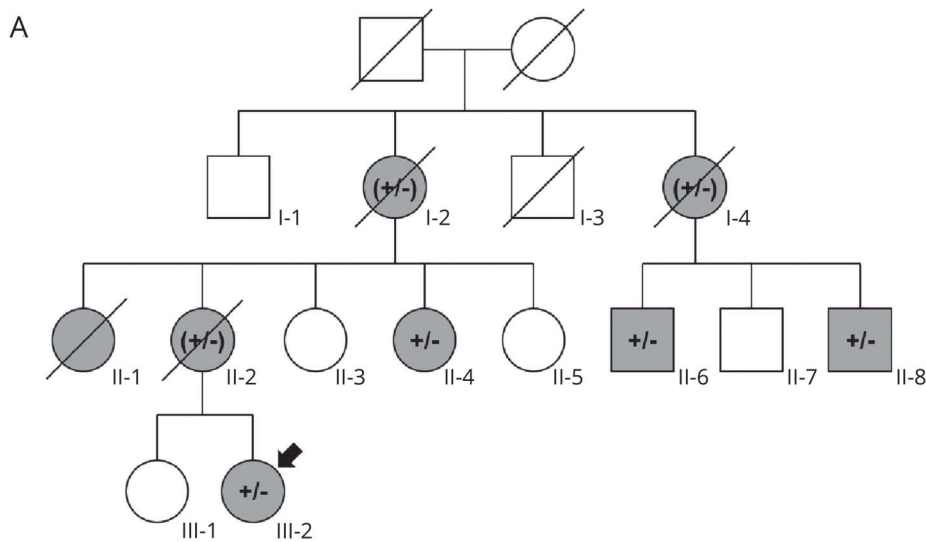
a score of 24/30 on the Mini-Mental State Examination, with striking deficits in attention and upon executing more complex commands. Vital signs were normal. Neurologic examination of the cranial nerves was normal, as were funduscopy, sensory examination, strength, and reflexes in all 4 limbs, with absence of clear pyramidal and frontal signs. Gait was slightly broad-based. Small-amplitude myoclonic jerks were noted in the arms, legs, and fingers, which interfered with cerebellar testing, but there was no ataxia. She did not have tremor; muscle tone was normal. Speech was slow, with multifocal facial myoclonus both at rest and during speaking, and she displayed signs of neurogenic stuttering. Speech-induced dystonic facial contractions were infrequently seen.

Neuropsychological testing 3 months after initial evaluation showed mostly deficits in attention and executive functions and to a lesser extent in verbal memory (table e-1, <http://links.lww.com/WNL/A174>). EEG repeatedly showed a moderate increase in slow activity in the theta and delta range, as well as occasional low-amplitude, generalized spike-wave discharges with central maximum, without clear photosensitivity (figure 1B).

The family history revealed several patients with adult-onset psychiatric or neurodegenerative disorders (figure 1A); more details are provided in the supplementary text (<http://links.lww.com/WNL/A176>). The mother of the proband (II-2) had been hospitalized at age 47 because of anxiety and depression but subsequently developed epilepsy at age 48 and a progressive cognitive decline compatible with FTD, which led to her death at age 56. A maternal aunt (II-4) had depression and memory problems. Neuropsychological testing suggested a possible FTD with onset in her mid-50s (data not shown).

Adult-onset autosomal dominant PME was diagnosed and further examinations were focused on elucidating the underlying cause. Ophthalmologic examination was normal. Routine blood analysis (table e-2, <http://links.lww.com/WNL/A174>) did not reveal abnormalities, nor did testing of CSF including dementia biomarkers (table e-3, <http://links.lww.com/WNL/A174>). MRI of the brain revealed generalized cerebral and cerebellar atrophy, mostly in the bilateral parietal lobes (figure 1C) with concordant relative hypometabolism on FDG-PET imaging. Skin and muscle biopsy were normal as were mitochondrial enzyme activities in muscle. Genetic testing for autosomal dominant spinocerebellar ataxias (SCA1-2-3-6-7-17), dentatorubral-

Figure 1 Pedigree, neurophysiology, and brain imaging of the proband

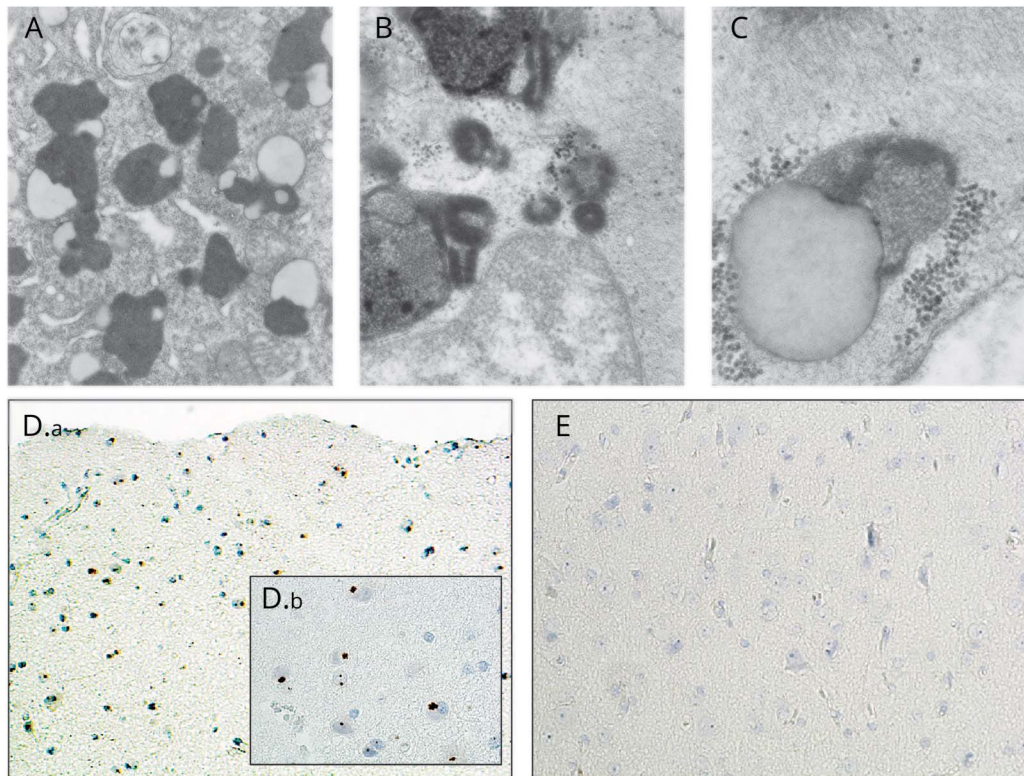


(A) Pedigree of the affected family. Shaded symbols denote affected family members; the proband is indicated with an arrow. Confirmed heterozygous *C9orf72* repeat expansions are shown as +/-; obligate carrier status is indicated as +/- (B) Representative EEG of the proband with a bilateral, synchronous epileptiform spike-wave discharge highlighted in gray. (C) Axial fluid-attenuated inversion recovery brain MRI of the proband demonstrates bilateral parietal lobe atrophy.

pallidolusian atrophy, Huntington disease, and familial Alzheimer disease (*PSEN1-2*, *APP*) was normal. Microarray-based comparative genomic hybridization did not reveal pathologic copy number variations. Whole exome sequencing (WES) of the patient and her maternal aunt was performed in the context of the ANCL Gene Discovery Consortium.¹² The WES dataset was filtered for variants in PME causative genes, namely *KCNC1*, *CERS1*, *PRICKLE1*, *EPM2A*, *GOSR2*, *KCTD7*, *LMNB2*, *NHLRC1*, *PRDM8*, *CSTB*, *SCARB2*, and *DNAJC5*,¹³ having a minor allele frequency <5% in the ExAC database. Using this approach, we did not detect any candidate variants in the proband. Additional searching for genetic alterations in a wider spectrum

of epilepsy genes¹⁴ did not reveal any potential candidate mutations.

Electron microscopy (EM) examination of a brain biopsy from the patient's right parietal lobe at age 34 showed some nonspecific increase in lipopigment (figure 2A), but no evidence of Lafora bodies or material diagnostic for NCL. EM analysis of the muscle biopsy of the maternal aunt (II-4) was more ambiguous and suggested presence of pathologic storage material in the form of lipopigment with occasional fingerprints (figure 2, B and C), although insufficient to establish a definite diagnosis of adult neuronal ceroid lipofuscinosis (ANCL) or Kufs disease. Subsequent expert review of the

Figure 2 Electron microscopy and immunohistochemistry

(A) Electron microscopy of the brain cortex of patient III-2 (proband) shows intraneuronal classical lipofuscin. (B, C) Electron microscopy of the skeletal muscle biopsy of patient II-4 demonstrates lipofuscin-like inclusions with fingerprints. (D.a, D.b) p62 staining in the brain cortex of patient III-2, with p62 positive cytoplasmic inclusions of different shape in some neurons and occasionally in glial cells. (E) Phospho-TDP-43 negative staining in the brain cortex. Magnifications $\times 27,000$ (A), $\times 67,500$ (B), $\times 107,500$ (C), $\times 4$ (D.a, E), and $\times 20$ (D.b).

biopsy findings within the same Consortium excluded the diagnosis of ANCL.

Next we tested for *C9orf72* repeat expansion, which was positive in both our patient and the affected aunt, as well as in 2 distant family members (II-6 and II-8) (figure 1A). Short-repeat PCR³ excluded a repeat size of less than 80 bp in the proband and her aunt. Further analysis of the brain biopsy with light microscopy examination showed clear neuronal cytoplasmic inclusions that stained positive for p62, but were negative for ubiquitin, TDP-43, and its hyperphosphorylated form (figure 2, D and E). Auto-fluorescence was slightly increased and ANCL-related staining for SCMAS, CathD, and LAMP2 were negative (figure e-1, <http://links.lww.com/WNL/A175>). Additional staining for amyloid, tau, FUS, and α -synuclein did not reveal pathologic changes (data not shown).

Discussion

We present a patient with PME and describe a remarkable association between this clinical syndrome and *C9orf72* repeat expansions. This constitutes an important finding for patients with PME of undetermined cause,² in particular because this type of intronic mutation cannot be identified through WES, as

was the case in our patient. *C9orf72* repeat expansions can be found in about 0.15⁹–0.2%¹⁵ of healthy individuals, but the absence of known PME-related defects in the WES data, and the segregation of the repeat expansion in the family, support a direct pathogenic role for the *C9orf72* repeat expansion in the PME phenotype of our patient.

Because of the autosomal dominant inheritance of adult-onset neuropsychiatric symptoms in family members, we focused our initial workup on the possibility of ANCL or Kufs disease causing PME in our patient. EM analysis of muscle tissue from the patient's maternal aunt also suggested an increase in pathologic lipofuscin-type deposits, but a definite diagnosis of ANCL could not be confirmed by the pathologists of the ANCL Consortium.¹² Mining publicly accessible databases with available data on *C9orf72* status^{9,16} did not reveal additional cases with symptoms suggestive of PME. Analysis of the patients with ANCL with autosomal dominant PME but without genetic diagnosis from the ANCL Consortium did not reveal other *C9orf72* repeat expansions ($n = 5$). Larger cohorts of patients with PME have not been tested.

This report supports the novel and emerging concept of disease anticipation in families segregating a *C9orf72* repeat expansion.¹⁷ Symptoms associated with *C9orf72* repeat

expansions typically manifest after the 4th decade,⁵ as illustrated by the proband's mother (II-2, onset around 47 years) and maternal aunt (II-4, onset around 55 years). Our patient had her first epileptic seizure more than 30 years earlier at age 15 and quickly thereafter developed progressive cognitive decline. Short-repeat PCR did not reveal the presence of short expansions in the proband or maternal aunt, and it is not yet possible to determine the exact length of longer repeat expansions. Although many factors may contribute to the clinical variation, one can speculate that meiotic repeat instability in the mother has resulted in a further expansion of the hexanucleotide repeat in the proband, resulting in the very early onset and atypical PME presentation.

It is intriguing to note that for a number of mid- to late-life inherited neurodegenerative diseases like Alzheimer disease,¹⁸ Huntington disease,¹⁹ neuroserpinopathy,²⁰ and dentatorubral-pallidoluyisian atrophy,²¹ classically presenting as dementias, the presentation can be of a PME when family members have an early onset. *C9orf72* repeat expansion can now be added to this list.

Our description of PME due to *C9orf72* repeat expansion expands the phenotypic spectrum associated with this intriguing noncoding hexanucleotide repeat expansion. Testing for this mutation should be considered in the workup of patients with PME, even when onset is in late childhood or adolescence.

Author contributions

Jelle van den Amelee: study concept and design, acquisition of data, analysis and interpretation, writing of the manuscript. Ivana Jedlickova: study concept and design, acquisition of data, analysis and interpretation, writing of the manuscript. Anna Pristoupilova: NGS data analysis and interpretation. Anne Sieben: acquisition of neuropathology data, critical revision of the manuscript. Sara Van Mossevelde: acquisition of data, critical revision of the manuscript. Chantal Ceuterick-de Groote: electron microscopy data acquisition, analysis and interpretation, critical revision of the manuscript. Helena Hůlková: acquisition of data, analysis and interpretation, critical revision of the manuscript. Radoslav Matej: acquisition of data, analysis and interpretation, critical revision of the manuscript. Alfred Meurs: EEG analysis and interpretation, critical revision of the manuscript. Christine Van Broeckhoven: acquisition of data, analysis and interpretation, critical revision of the manuscript. Samuel F. Berkovic: study supervision, acquisition of data, analysis and interpretation, critical revision of the manuscript. Patrick Santens: study concept and design, study supervision, acquisition of data, analysis and interpretation, writing of the manuscript. Stanislav Kmoch: study concept and design, study supervision, acquisition of data, analysis and interpretation, writing of the manuscript. Bart Dermaut: study concept and design, study supervision, acquisition of data, analysis and interpretation, writing of the manuscript.

Acknowledgment

The authors thank the patients and family members for their participation; the Genomic facility in Motol University

Hospital in Prague (OPPK.CZ.2.16/3.100/24022) and The National Center for Medical Genomics (LM2015091) for their instrumental and technical support with exome sequencing and data analyses; and Marleen Praet, Martin Lammens, Elfride De Baere, Kathleen Claes, Miet De Letter, Isabelle Leber, Anne De Septenville, Celine Bellenguez, Marleen Van den Broeck, Jean-Jacques Martin, John Staropoli, and Sara Mole for their help and suggestions.

Study funding

I.J., A.P., and S.K. are supported by grants 269615 from the Charles University Grant Agency and 14-36804 G from the Grant Agency of the Czech Republic. Institutional support was provided by Charles University institutional programs PRVOUK-P24/LF1/3, UNCE 204011, and SVV2017/260367, and by the project LQ1604 NPU II from the Ministry of Education, Youth and Sports of the Czech Republic. R. M. and H.H. are supported by project of the Ministry of Health, Czech Republic (Conceptual development of research organization 64165, General University Hospital in Prague) and by Charles University (Project Progres Q28/LF1). C.V.B. is supported by the Interuniversity Attraction Poles program P7/16 of the Belgian Science Policy Office (BELSPO), the Flemish initiated Impulse Program on Networks for Dementia Research (VIND), and the Flemish government initiated Methusalem Excellence Program. B.D. is supported by the Interuniversity Attraction Poles program P7/16 of the Belgian Science Policy Office (BELSPO), Inserm, the Université de Lille, the Fondation Plan Alzheimer, the LABEX (laboratory of excellence program investment for the future) DISTALZ grant (Development of Innovative Strategies for a Transdisciplinary approach to Alzheimer's disease) and INSTALZ, an EU Joint Programme—Neurodegenerative Disease Research (JPND) project. The INSTALZ project is supported through the following funding organizations under the aegis of JPND (Belgium, Research Foundation Flanders; Denmark, Innovation Fund Denmark; France, Agence Nationale de la Recherche; Sweden, Swedish Research Council; United Kingdom, Medical Research Council). The project has received funding from the European Union's Horizon 2020 research and innovation programme under grant agreement 643417.

Disclosure

J. van den Amelee, I. Jedlickova, A. Pristoupilova, A. Sieben, S. Van Mossevelde, C. Ceuterick-de Groote, H. Hůlková, and R. Matej report no disclosures relevant to the manuscript. A. Meurs received honoraria from serving on the advisory board of UCB and GSK and received speaker's fees and funding for a trip from UCB. C. Van Broeckhoven, S. Berkovic, P. Santens, S. Kmoch, and B. Dermaut report no disclosures relevant to the manuscript. Go to Neurology.org/N for full disclosures.

Received July 13, 2017. Accepted in final form November 14, 2017.



References

1. Marseille Consensus Group. Classification of progressive myoclonus epilepsies and related disorders. *Ann Neurol* 1990;28:113–116.

2. Franceschetti S, Michelucci R, Canafoglia L, et al. Progressive myoclonic epilepsies definitive and still undetermined causes. *Neurology* 2014;82:405–411.
3. Gijssels I, Cruts M, Van Broeckhoven C. The genetics of C9orf72 expansions. *Cold Spring Harb Perspect Med Epub* 2017 Jan 27.
4. Gijssels I, Van Mossevelde S, van der Zee J, et al. The C9orf72 repeat size correlates with onset age of disease, DNA methylation and transcriptional downregulation of the promoter. *Mol Psychiatry* 2015;21:1–13.
5. Gijssels I, Van Langenhove T, van der Zee J, et al. A C9orf72 promoter repeat expansion in a Flanders-Belgian cohort with disorders of the frontotemporal lobar degeneration-amyotrophic lateral sclerosis spectrum: a gene identification study. *Lancet Neurol* 2012;11:54–65.
6. Renton AE, Majounie E, Waite A, et al. A hexanucleotide repeat expansion in C9ORF72 is the cause of chromosome 9p21-linked ALS-FTD. *Neuron* 2011;72:257–268.
7. DeJesus-Hernandez M, Mackenzie IR, Boeve BF, et al. Expanded GGGGCC hexanucleotide repeat in noncoding region of C9ORF72 causes chromosome 9p-linked FTD and ALS. *Neuron* 2011;72:245–256.
8. Rohrer JD, Isaacs AM, Mizlienska S, et al. C9orf72 expansions in frontotemporal dementia and amyotrophic lateral sclerosis. *Lancet Neurol* 2015;14:291–301.
9. Beck J, Poulter M, Hensman D, et al. Large C9orf72 hexanucleotide repeat expansions are seen in multiple neurodegenerative syndromes and are more frequent than expected in the UK population. *Am J Hum Genet* 2013;92:345–353.
10. Vatsavayai SC, Yoon SJ, Gardner RC, et al. Timing and significance of pathological features in C9orf72 expansion-associated frontotemporal dementia. *Brain* 2016;139:3202–3216.
11. Capasso M, Anzellotti F, Di Giacomo R, Onofrij M. Epilepsy and electroencephalographic abnormalities in C9orf72 repeat expansion. *Amyotroph Lateral Scler Frontotemporal Degener* 2017;18:140–141.
12. Berkovic SF, Staropoli JF, Carpenter S, et al. Diagnosis and misdiagnosis of adult neuronal ceroid lipofuscinosis (Kufs disease). *Neurology* 2016;87:579–584.
13. Nosková L, Stránecký V, Hartmannová H, et al. Mutations in DNAJCS, encoding cysteine-string protein alpha, cause autosomal-dominant adult-onset neuronal ceroid lipofuscinosis. *Am J Hum Genet* 2011;89:241–252.
14. Wang J, Lin Z-J, Liu L, et al. Epilepsy-associated genes. *Seizure* 2017;44:11–20.
15. Majounie E, Renton AE, Mok K, et al. Frequency of the C9orf72 hexanucleotide repeat expansion in patients with amyotrophic lateral sclerosis and frontotemporal dementia: a cross-sectional study. *Lancet Neurol* 2012;11:323–330.
16. Keogh MJ, Wei W, Wilson I, et al. Genetic compendium of 1511 human brains available through the UK medical research Council brain banks network resource. *Genome Res* 2017;27:165–173.
17. Van Mossevelde S, van der Zee J, Gijssels I, et al. Clinical evidence of disease anticipation in families segregating a C9orf72 repeat expansion. *JAMA Neurol Epub* 2017 Feb 13.
18. Melanson M, Nalbantoglu J, Berkovic S, et al. Progressive myoclonus epilepsy in young adults with neuropathologic features of Alzheimer's disease. *Neurology* 1997;49:1732–1733.
19. Gambardella A, Muglia M, Labate A, et al. Juvenile Huntington's disease presenting as progressive myoclonic epilepsy. *Neurology* 2001;57:708–711.
20. Davis RL, Shrimpton AE, Carrell RW, et al. Association between conformational mutations in neuroserpin and onset and severity of dementia. *Lancet* 2002;359:2242–2247.
21. Iizuka R, Hirayama K, Maehara KA. Dentato-rubro-pallido-luysian atrophy: a clinico-pathological study. *J Neurol Neurosurg Psychiatry* 1984;47:1288–1298.



Autosomal-dominant adult neuronal ceroid lipofuscinosis caused by duplication in *DNAJC5* initially missed by Sanger and whole-exome sequencing

Ivana Jedličková¹ · Maxime Cadieux-Dion ^{2,3} · Anna Přistoupilová¹ · Viktor Stránecký¹ · Hana Hartmannová¹ · Kateřina Hodaňová¹ · Veronika Barešová¹ · Helena Hůlková^{1,4} · Jakub Sikora ^{1,4} · Lenka Nosková¹ · Dita Mušálková¹ · Petr Vyleťal¹ · Jana Sovová¹ · Patrick Cossette² · Eva Andermann⁵ · Frederick Andermann⁵ · Stanislav Kmoč¹ · The Adult NCL Gene Discovery Consortium

Received: 3 May 2019 / Revised: 29 November 2019 / Accepted: 10 December 2019 / Published online: 9 January 2020
© The Author(s), under exclusive licence to European Society of Human Genetics 2020

Abstract

Adult-onset neuronal ceroid lipofuscinoses (ANCL, Kufs disease) are rare hereditary neuropsychiatric disorders characterized by intralysosomal accumulation of ceroid in tissues. The ceroid accumulation primarily affects the brain, leading to neuronal loss and progressive neurodegeneration. Although several causative genes have been identified (*DNAJC5*, *CLN6*, *CTSF*, *GRN*, *CLN1*, *CLN5*, *ATP13A2*), the genetic underpinnings of ANCL in some families remain unknown. Here we report one family with autosomal dominant (AD) Kufs disease caused by a 30 bp in-frame duplication in *DNAJC5*, encoding the cysteine-string protein alpha (CSP α). This variant leads to a duplication of the central core motif of the cysteine-string domain of CSP α and affects palmitoylation-dependent CSP α sorting in cultured neuronal cells similarly to two previously described CSP α variants, p.(Leu115Arg) and p.(Leu116del). Interestingly, the duplication was not detected initially by standard Sanger sequencing due to a preferential PCR amplification of the shorter wild-type allele and allelic dropout of the mutated *DNAJC5* allele. It was also missed by subsequent whole-exome sequencing (WES). Its identification was facilitated by reanalysis of original WES data and modification of the PCR and Sanger sequencing protocols. Independently occurring variants in the genomic sequence of *DNAJC5* encoding the cysteine-string domain of CSP α suggest that this region may be more prone to DNA replication errors and that insertions or duplications within this domain should be considered in unsolved ANCL cases.

These authors contributed equally: Ivana Jedličková, Maxime Cadieux-Dion

Supplementary information The online version of this article (<https://doi.org/10.1038/s41431-019-0567-2>) contains supplementary material, which is available to authorized users.

✉ Stanislav Kmoč
skmoch@lf1.cuni.cz

- ¹ Research Unit for Rare Diseases, Department of Pediatrics and Adolescent Medicine, First Faculty of Medicine, Charles University, Prague, Czech Republic
- ² Centre Hospitalier de L'Université de Montréal, Montréal, QC, Canada
- ³ Center for Pediatric Genomic Medicine, Children's Mercy Hospital, Kansas City, MO, USA
- ⁴ Institute of Pathology, First Faculty of Medicine and General University Hospital, Charles University, Prague, Czech Republic
- ⁵ Montreal Neurological Hospital & Institute, McGill University, Montreal, QC, Canada

Introduction

Adult-onset neuronal ceroid lipofuscinoses (ANCL) constitute a group of rare genetic diseases characterized clinically by the progressive deterioration of mental and motor functions and histopathologically by the intracellular and ultrastructurally distinct accumulation of autofluorescent lipopigment—ceroid—in the brain and other tissues. Age of onset, spectrum of neurological phenotypes, and disease progression can vary even within families. Clinical heterogeneity of ANCLs is in line with diverse inheritance patterns, increasing number of identified causal genes (e.g., *DNAJC5* [1], *CLN6* [2], *CTSF* [3], *GRN* [4], *CLN1* [5], *CLN5* [6], *ATP13A2* [7]), and various types of causative variants and their combinations (NCL Resource—A Gateway for Batten Disease: http://www.ucl.ac.uk/ncl/new_nomenclature.shtml).

Diagnosis of ANCLs is challenging from a clinical, histopathologic, as well as diagnostic perspective. Even

with recent technological advances [8, 9], the causative genetic variant(s) in some ANCL families have not been identified. In order to improve genetic diagnosis in these families, we recently established The Adult NCL Gene Discovery Consortium. Within the Consortium we reviewed clinical and histopathological data and classified recruited cases as definite, probable, or possible ANCL or not meeting the diagnostic criteria for ANCL [10]. ANCL cases were then subjected to candidate gene and whole-exome sequencing (WES) [11, 12].

Here we report and characterize a new variant—a **30 base pair in-frame duplication** in *DNAJC5*, that we have identified in one of the investigated ANCL families. The identification of this variant was particularly challenging. It was initially missed by Sanger sequencing of *DNAJC5* and WES, to be identified later by reanalysis of original WES data that were shared within the Consortium. Our work thus also provides a cautionary tale about the challenges in identification of even relatively short insertions and duplications by standard genetic methods.

Materials and methods

Subjects

The study protocol was approved by the local Institutional Review Boards and signed informed consent was obtained from all subjects.

The Canadian family was ascertained at the Montreal Neurological Institute, McGill University, Canada based on clinical observation of three affected individuals: a mother and two sons. The mother was diagnosed with Kufs disease at the age of 42 and died at the age of 56 (no clinical details are available). The affected sons presented with seizures, memory loss, and disability (wheelchair bound) at the age of 31 and 34. No biopsy material for pathological evaluation was available at the time of investigation to examine for the presence of typical lipopigment in tissues of affected individuals.

DNA sequencing and variant analysis

Genomic DNA of the two brothers was extracted from whole blood samples by a standard protocol. Coding regions of *DNAJC5* (NG_029805.2) were amplified by PCR from genomic DNA of the two brothers and sequenced by direct Sanger sequencing using the version 3.1 Dye Terminator cycle sequencing kit (ThermoFisher Scientific) with electrophoresis on an ABI 3500XL Avant Genetic Analyzer (ThermoFisher Scientific). Data were analyzed using Sequencing Analysis software (ThermoFisher Scientific).

Exome sequencing

Exome sequencing was performed using genomic DNA from the two affected brothers (Fig. 1). For DNA enrichment, the Sure Select Human All Exon V4 capture kit (Agilent Technologies, Santa Clara, CA) was used according to the manufacturer's protocol. DNA sequencing was performed on the captured barcoded DNA library via an Illumina HiSeq 2000 system as a pair end library with the read length of 100 bp. The resulting FASTQ files were aligned to the human reference genome (hg19) via BWA-MEM [13]. After genome alignment, conversion of SAM format to BAM and duplicate removal were performed using Picard Tools (1.129). The Genome Analysis Toolkit, GATK (3.2.2) [14–16] was used for local realignment around indels, base recalibration, variant recalibration, and variant calling (HaplotypeCaller). Variant annotation was performed with SnpEff 3.6 [17] and GEMINI 0.18.2 [18].

In silico analysis of the cysteine-string domain

Hydrophobicity and palmitoylation potential of the wild-type (wt) cysteine-string domain (CSD) and the CSD carrying the *DNAJC5* variant were analyzed with a Kyte–Doolittle algorithm and CSS-Palm 2.0, respectively, as described previously [1].

CSP α -expression vectors

DNAJC5/CSP α cDNA was amplified by RT-PCR from the affected individuals' leukocytes with specific primers. Resulting PCR products were first cloned into PCR2.1 TOPO TA-cloning vector (Invitrogen) and, after sequencing verification, the cDNA region containing the 30 bp duplication was subcloned into a pEGFP-C1/*DNAJC5* wt vector using BstXI and BsmBI restriction sites. The pEGFP-C1/*DNAJC5*_wt, pEGFP-C1/*DNAJC5*_Leu115Arg, and pEGFP-C1/*DNAJC5*_Leu116del vectors were generated as described previously [1].

Transient expression of EGFP–CSP α

cDNA constructs were transfected into CAD5 cells derived from Cath. -a-differentiated (CAD) cells (provided by Sukhvir Mahal, The Scripps Research Institute, Jupiter, FL, USA). Four to seven days before transfection, 1×10^4 cells/cm² were seeded with Opti-MEM medium (Opti-MEM; Invitrogen) containing 10% FBS (HyClone, Logan, UT), 90 units penicillin, streptomycin/ml. Cells were transfected by either 0.8 or 4 μ g of plasmid constructs with Lipofectamine 2000 (Invitrogen) in serum and antibiotics free Opti-MEM medium according to the

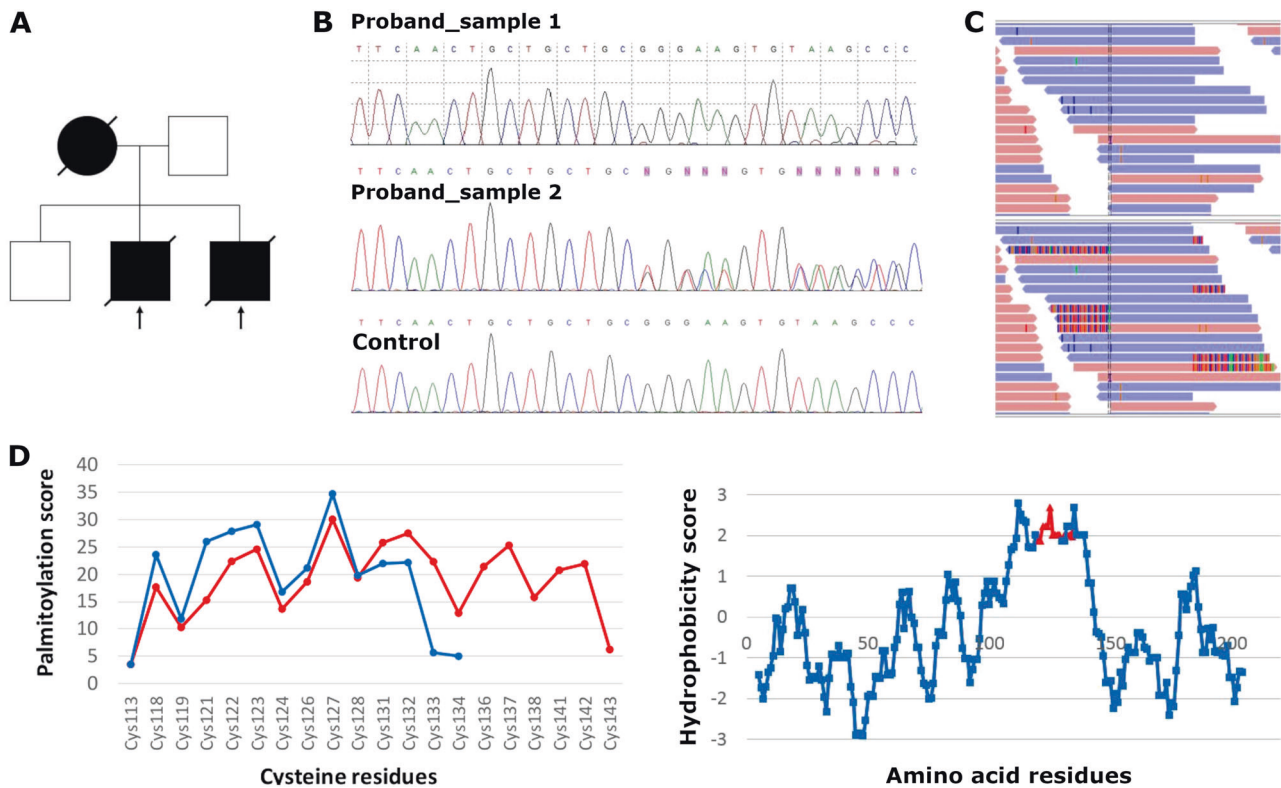


Fig. 1 Sanger sequencing and reads alignment of the *DNAJC5* bearing the 30 bp duplication. a Pedigree of the Canadian family suggesting an autosomal dominant inheritance. **b** Chromatograms of *DNAJC5* genomic DNA sequences showing normal *DNAJC5* sequence in the proband using original protocol (Proband_sample 1) and heterozygous duplication in the same DNA sample upon modified PCR protocol (Proband_sample 2). Lower panel shows chromatogram from control DNA. **c** The 30 bp duplication in *DNAJC5* in the

Integrative Genomics Viewer (IGV2.3) before (upper panel) and after a visualization of soft-clipped bases (lower panel). **d** In silico analysis of the cysteine-string domain showing that compared with the wild-type sequence (blue line), the duplication (red line) alters palmitoylation potential (left panel) and hydrophobicity profile (right panel), critical parameters of post-translational modification, and intracellular localization of CSP α .

manufacturer's protocol. Transfection experiments were performed in more than three replicates.

Immunofluorescence analysis

Cells were fixed 24 h after transfection with chilled methanol for 10 min, washed, blocked with 5% bovine serum albumin (BSA), and incubated for 1 h at 37 °C with antiprotein disulfide isomerase mouse monoclonal IgG1 (Stressgen, San Diego, CA) for endoplasmic reticulum (ER) localization, anti-GS28 mouse IgG1 (Stressgen, San Diego, CA) for Golgi localization, and anti-GFP rabbit polyclonal IgG (Abcam) for EGFP-CSP α detection. For fluorescence detection, corresponding species-specific secondary antibodies Alexa Fluor 488 and Alexa Fluor 555 (Molecular Probes, Invitrogen, Paisley, UK) were used. Prepared slides were mounted in ProLong[®] Gold Antifade with 4',6-diamidino-2-phenylindole staining nuclei (Life Technologies, Foster City, USA) fluorescence mounting medium and analyzed by confocal microscopy.

Image acquisition and analysis

Prepared slides were analyzed by confocal microscopy. XYZ images were sampled according to Nyquist criterion using a LeicaSP8X laser scanning confocal microscope, HC PL APO objective (63 \times , N.A. 1.40), 405, 488, and 543 laser lines. Images were restored using a classic maximum likelihood restoration algorithm in the Huygens Professional Software (SVI, Hilversum, The Netherlands) [19]. The colocalization maps employing single pixel overlap coefficient values ranging from 0 to 1 were created in the Huygens Professional Software [20]. The resulting overlap coefficient values are presented as the pseudo color denoted in the corresponding lookup tables.

Immunoblot analysis

Transfected CAD5 cells were harvested in PBS, centrifuged at 610 \times g for 5 min, resuspended in 50 mM Tris pH 6.8, 50 mM DTT, 2% sodium dodecyl sulfate (SDS), and Complete Protease Inhibitor Cocktail (Roche) or PBS with

Triton X-100, 0.1 or 0.5% and Complete Protease Inhibitor Cocktail (Roche), homogenized by sonication using the Covaris S2 Ultrasonicator, followed by denaturation at 100 °C for 10 min. The protein content in the supernatant was determined using an infrared spectrometer Direct Detect infrared (Millipore) according to the manufacturer's protocol. Protein lysates equivalent to 15 or 20 µg of protein were incubated with and without 6 M hydroxylamine for CSPα depalmitoylation for 24 h at room temperature and reduced at 100 °C for 5 min in sample buffer with or without 1% beta-mercaptoethanol (βME) before SDS-PAGE electrophoresis. After protein transfer to the polyvinylidene fluoride membrane, membranes were blocked by 5% milk and 0.1% Tween 20 in PBS over night at 4 °C. CSPα or CSPα-EGFP protein was visualized by incubation with rabbit CSP antibody (Stressgen) at 1:5000 in 0.1% BSA and 0.1% Tween 20 in PBS for 60 min or rabbit green fluorescent protein (GFP) antibody (Abcam) at 1:3000 in 0.1% BSA and 0.1% Tween 20 in PBS for 60 min, followed by incubation with goat antirabbit HRP (Pierce) at 1:10,000 in 0.1% Tween 20 in PBS for 60 min and detection by Clarity Western ECL Substrate (Bio-Rad).

Results

Identification of 30 base pair duplication in *DNAJC5* by a combination of exome sequencing and sanger sequencing

To identify the genetic lesion in affected family members we initially Sanger sequenced and excluded *DNAJC5*, the prevalent gene for autosomal dominant ANCL (AD-ANCL) (Fig. 1b). Next we sequenced all coding exons and 5' and 3' untranslated regions of their corresponding mRNAs (UTRs) (Sure Select Human All Exon V4 capture kit, Illumina HiSeq 2000) in both affected brothers. Considering an autosomal dominant model of inheritance, we searched for variants that had standard read count threshold ≥ 10 , were present in the heterozygous state in both affected individuals and had a minor allele frequency $< 0.5\%$ in The Exome Aggregation Consortium database [21]. These parameters did not yield any functionally relevant candidate variant. Lowering the standard read count threshold to ≥ 5 , we found a 30 bp in-frame duplication in *DNAJC5*. This variant was however not seen in the IGV tool, which allows visualization of sequence alignments. Essential for the variant detection was a visualization of so called soft-clipped bases, which are reads not matching with the reference sequence in their whole length. Using the visualization of soft-clipped bases we revealed the 30 bp in-frame duplication: chr20:g.62562252_62562281dup (hg19); NM_025219.2:c.370_399dup (p.(Cys124_Cys133dup)), in

exon 4 of *DNAJC5*. (Fig. 1c). We modified our original PCR protocol and confirmed the presence of the duplication using standard Sanger sequencing (Fig. 1a, upper panels). The variant was submitted to ClinVar database under the accession code VCV000689476 and to the Mutation and Patient Database for Human NCL genes [22].

In silico analysis of the novel CSPα c.370_399dup (p.(Cys124_Cys133dup)) variant

The duplication encodes for a duplication of the central core motif of the CSD of CSPα. NM_025219.2:c.370_399dup (p.(Cys124_Cys133dup)). The CSD is implicated in palmitoylation and membrane trafficking of CSPα. In silico analysis suggested that the duplication increases hydrophobicity (Fig. 1d, right panel) of the CSD and that the presence of the additional seven cysteine residues changes the palmitoylation potential (Fig. 1d, left panel). Changes in these parameters can make the protein carrying the p.(Cys124_Cys133dup) variant prone to aggregation [23].

The functional effect of the GFP-tagged CSPα p.(Cys124_Cys133dup) variant in neuronal CAD5 cell model

To assess the effect of the identified duplication on CSPα expression and intracellular localization we transiently expressed N-terminal GFP tagged CSPα with the identified duplication p.(Cys124_Cys133dup), wt CSPα (GFP_CSPα_wt) and GFP_CSPα with previously identified variants NM_025219.2:c.344T>G (p.(Leu115Arg)) and NM_025219.2:c.343_345del (p.(Leu116del)), both variants located in exon 4 of *DNAJC5* (the exon numbering starts with exon 1 to exon 5), shortly p.(Leu115Arg) and p.(Leu116del), in CAD5 cells. Immunofluorescence analysis and colocalization studies showed that the GFP_CSPα_wt and the endogenous CSPα are localized dominantly along the plasma membrane in finely granular cytoplasmic structures. All three GFP_CSPα proteins with the variants p.(Cys124_Cys133dup), p.(Leu115Arg), and p.(Leu116del) had reduced expression on the plasma membrane. They are present mostly in cytoplasm, either in a diffuse form or as a coarsely granular inclusions that colocalize to a certain extent with markers of ER and Golgi apparatus (Fig. 2, Supplementary Fig. 1).

Immunoblot analysis of GFP-CSPα transiently produced in CAD5 cells

To assess the effect of the identified duplication we performed western blot analysis of transiently transfected CAD5 cell lysates before and after chemical depalmitoylation performed under different denaturing conditions

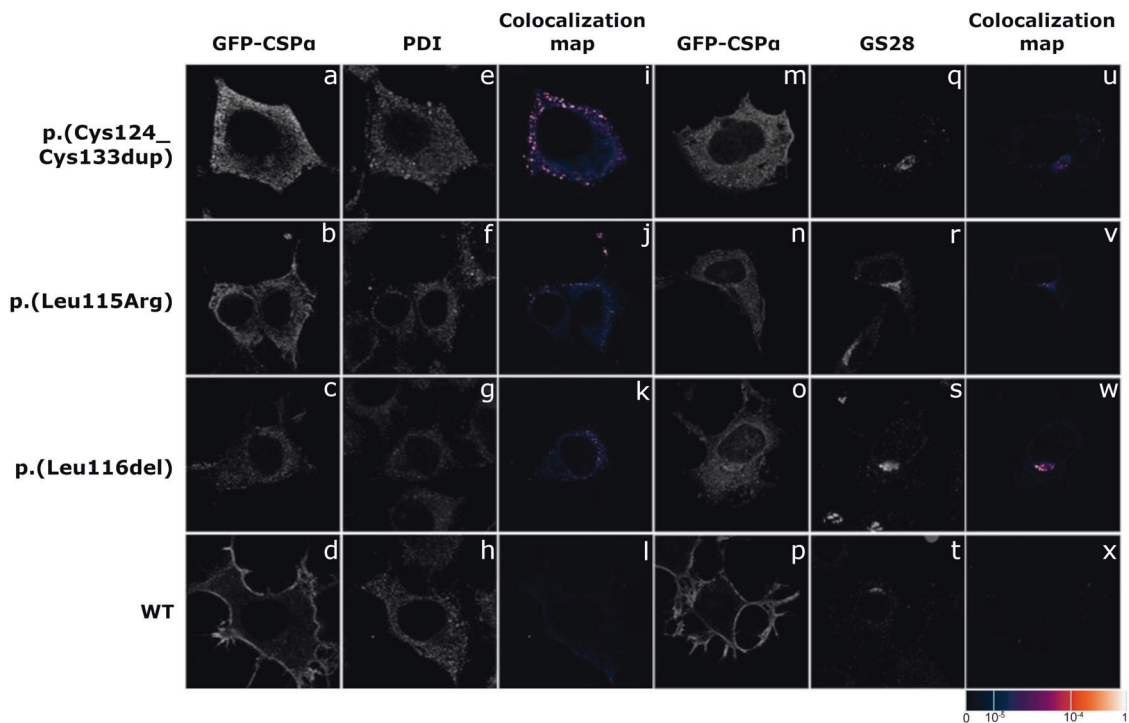


Fig. 2 Immunofluorescence analysis of transiently expressed GFP-tagged CSP α wt and variant proteins in CAD5 cells. All three variant proteins (**a–c**, **m–o**) are present in a finely or coarsely granular structures. Co-staining with (**e–g**) protein disulfide isomerase (PDI), a marker of endoplasmic reticulum (ER), and (**q–s**) Golgi SNAP receptor complex member 1 (GS28) demonstrates abnormal presence

(Fig. 3). We found that the GFP_CSP α protein carrying the Cys124_Cys133dup is present exclusively in non-palmitoylated form, whereas GFP_CSP α _Leu115Arg and GFP_CSP α _Leu116del proteins can present in both, the nonpalmitoylated or palmitoylated CSP α with the former more abundant. All three GFP_CSP α _Leu115Arg, GFP_CSP α _Leu116del, and GFP_CSP α _Cys124_Cys133dup proteins formed high molecular weight aggregates that were resistant to SDS and reducing agents (DTT, β ME). The aggregates became soluble by these procedures only upon initial chemical depalmitoylation by hydroxylamine (Fig. 3).

Discussion

In this work we identified a 30 bp duplication in *DNAJC5* encoding CSP α in one family ascertained by The Adult NCL Gene Discovery Consortium. The variant leads to a duplication of the central core motif of the CSD and affects palmitoylation-dependent CSP α sorting in cultured neuronal cells similar to two other previously described single nucleotide CSP α variants p.Leu115Arg and p.Leu116del. CSP α acts as a co-chaperone in the formation of presynaptic SNARE complexes (soluble N-ethylmaleimide-sensitive

of mutated proteins in ER (**i–k**) and Golgi (**u–w**). Wild-type protein (**d**, **h**, **l**, **p**, **t**, **x**) is present exclusively on plasma membrane. The degree of colocalization of GFP_CSP α with selected markers is demonstrated by the fluorescent signal overlap coefficient values ranging from 0 to 1. The resulting overlap coefficient values are presented as the pseudo color whose scale is shown in corresponding lookup table.

factor attachment protein receptors) [24]. The SNAREs are essential for docking of synaptic vesicles, their fusion and recycling. There is accumulating evidence that disruption of the SNARE machinery leads to neurodegeneration [25].

This family remained genetically undefined for decades. Initially, the variant could not be detected by standard Sanger sequencing of *DNAJC5* probably due to a preferential PCR amplification of the shorter wt allele and allelic dropout of the mutated *DNAJC5* allele. It was also missed by a subsequent analysis of WES. Its identification was facilitated by reanalysis of the original WES data shared within the Consortium and modification of the PCR and Sanger sequencing protocols.

Independently occurring variants in the genomic sequence of *DNAJC5* encoding the CSD of CSP α [1] suggest that this region may be more prone to DNA replication errors and that insertions or duplications within this domain should be considered in not yet solved ANCL cases.

Our work demonstrates the limitations of Sanger sequencing and WES in detection of even relatively small insertions and duplications and shows that analysis of next generation sequence data still requires an individualized approach and unique interpretations of the data. Continued reanalysis of the data with a team of experienced scientists

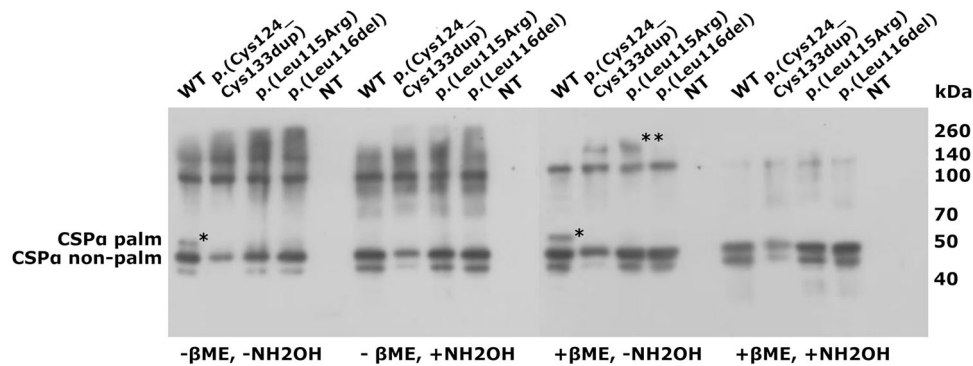


Fig. 3 Immunoblot analysis of transiently expressed GFP-tagged CSP α proteins in CAD5 cells. Immunodetection using the CSP antibody reveals that the GFP_CSP α _p.(Cys124_Cys133dup) protein is present exclusively in nonpalmitoylated form (CSP α nonpalm; the asterisk (*) refers to the palmitoylated form—CSP α palm). All three GFP_CSP α proteins with the variants p.(Leu115Arg), p.(Leu116del), p.(Cys124_Cys133dup) form high molecular weight aggregates (**) resistant to sodium dodecyl sulfate (SDS) and reducing agents (DTT, β ME). The aggregates are soluble only upon initial chemical depalmitoylation by hydroxylamine (NH₂OH).

may identify previously missed variants. Approximately 75% of patients with neurodegeneration subjected to WES remain without a genetic diagnosis [26]. It is unclear how many similar variants will be identified by continued reanalysis, as demonstrated in this paper.

Data availability

The authors state that anonymized data will be shared by request from any qualified investigator.

Acknowledgements This work was supported by Ministry of Health of the Czech Republic, grant nr. NV19-08-137. Institutional support was provided by Charles University institutional programs PRVOUK-P24/LF1/3, UNCE 204064, and SVV2016/260148, by the project LQ1604 NPU II from the Ministry of Education, Youth and Sports of the Czech Republic. We thank The National Center for Medical Genomics (LM2015091) for their instrumental and technical support with the WES analyses. Instrumental support was provided by grant CZ.1.05/2.1.00/19.0400 from the Research and Development for Innovations Operational Programme (RDIOP) cofinanced by European regional development fund and the state budget of the Czech Republic.

Compliance with ethical standards

Conflict of interest The authors declare that they have no conflict of interest.

Publisher's note Springer Nature remains neutral with regard to jurisdictional claims in published maps and institutional affiliations.











References

- Noskova L, Stranecky V, Hartmannova H, Pristoupilova A, Baresova V, Ivanek R, et al. Mutations in DNAJC5, encoding cysteine-string protein alpha, cause autosomal-dominant adult-onset neuronal ceroid lipofuscinosis. *Am J Hum Genet.* 2011;89:241–52.
- Arsov T, Smith KR, Damiano J, Franceschetti S, Canafoglia L, Bromhead CJ, et al. Kufs disease, the major adult form of neuronal ceroid lipofuscinosis, caused by mutations in CLN6. *Am J Hum Genet.* 2011;88:566–73.
- Smith KR, Dahl HH, Canafoglia L, Andermann E, Damiano J, Morbin M, et al. Cathepsin F mutations cause Type B Kufs disease, an adult-onset neuronal ceroid lipofuscinosis. *Hum Mol Genet.* 2013;22:1417–23.
- Smith KR, Damiano J, Franceschetti S, Carpenter S, Canafoglia L, Morbin M, et al. Strikingly different clinicopathological phenotypes determined by progranulin-mutation dosage. *Am J Hum Genet.* 2012;90:1102–7.
- van Diggelen OP, Thobois S, Tilikete C, Zabet MT, Keulemans JL, van Bunderen PA, et al. Adult neuronal ceroid lipofuscinosis with palmitoyl-protein thioesterase deficiency: first adult-onset patients of a childhood disease. *Ann Neurol.* 2001;50:269–72.
- Xin W, Mullen TE, Kiely R, Min J, Feng X, Cao Y, et al. CLN5 mutations are frequent in juvenile and late-onset non-Finnish patients with NCL. *Neurology.* 2010;74:565–71.
- Bras J, Verloes A, Schneider SA, Mole SE, Guerreiro RJ. Mutation of the parkinsonism gene ATP13A2 causes neuronal ceroid lipofuscinosis. *Hum Mol Genet.* 2012;21:2646–50.
- Cotman SL, Karaa A, Staropoli JF, Sims KB. Neuronal ceroid lipofuscinosis: impact of recent genetic advances and expansion of the clinicopathologic spectrum. *Curr Neurol Neurosci Rep.* 2013;13:366.
- Kmoch S, Stranecky V, Emes RD, Mitchison HM. Bioinformatic perspectives in the neuronal ceroid lipofuscinoses. *Biochim Biophys Acta.* 2013;1832:1831–41.
- Berkovic SF, Staropoli JF, Carpenter S, Oliver KL, Kmoch S, Anderson GW, et al. Diagnosis and misdiagnosis of adult neuronal ceroid lipofuscinosis (Kufs disease). *Neurology.* 2016;87:579–84.
- Ehling R, Noskova L, Stranecky V, Hartmannova H, Pristoupilova A, Hodanova K, et al. Cerebellar dysfunction in a family harboring the PSEN1 mutation co-segregating with a cathepsin D variant p.A58V. *J Neurol Sci.* 2013;326:75–82.
- van den Aemele J, Jedlickova I, Pristoupilova A, Sieben A, Van Mossevelde S, Ceuterick-de Groote C, et al. Teenage-onset progressive myoclonic epilepsy due to a familial C9orf72 repeat expansion. *Neurology.* 2018;90:e658–e663.
- Li H. Aligning sequence reads, clone sequences and assembly contigs with BWA-MEM. *Bioinformatics.* 2013;00:1–2.

14. McKenna A, Hanna M, Banks E, Sivachenko A, Cibulskis K, Kernytsky A, et al. The Genome Analysis Toolkit: a MapReduce framework for analyzing next-generation DNA sequencing data. *Genome Res.* 2010;20:1297–303.
15. DePristo MA, Banks E, Poplin R, Garimella KV, Maguire JR, Hartl C, et al. A framework for variation discovery and genotyping using next-generation DNA sequencing data. *Nat Genet.* 2011;43:491–8.
16. Van der Auwera GA, Carneiro MO, Hartl C, Poplin R, Del Angel G, Levy-Moonshine A, et al. From FastQ data to high confidence variant calls: the Genome Analysis Toolkit best practices pipeline. *Curr Protoc Bioinform.* 2013;43:11 10 1–33.
17. Cingolani P, Platts A, Wang le L, Coon M, Nguyen T, Wang L, et al. A program for annotating and predicting the effects of single nucleotide polymorphisms, SnpEff: SNPs in the genome of *Drosophila melanogaster* strain w1118; iso-2; iso-3. *Fly.* 2012;6:80–92.
18. Paila U, Chapman BA, Kirchner R, Quinlan AR. GEMINI: integrative exploration of genetic variation and genome annotations. *PLoS Comput Biol.* 2013;9:e1003153.
19. Landmann L. Deconvolution improves colocalization analysis of multiple fluorochromes in 3D confocal data sets more than filtering techniques. *J Microsc.* 2002;208(Pt 2):134–47.
20. Manders EMM, Verbeek FJ, Aten JA. Measurement of colocalization of objects in dual-color confocal images. *J Microsc.* 1993;169:375–82.
21. Lek M, Karczewski KJ, Minikel EV, Samocha KE, Banks E, Fennell T, et al. Analysis of protein-coding genetic variation in 60,706 humans. *Nature.* 2016;536:285–91.
22. Mole SE, Gardener E. Mutation and patient database for human NCL genes. 2019. <https://www.ucl.ac.uk/ncl-disease/mutation-and-patient-database/mutation-and-patient-datasheets-human-ncl-genes>. Accessed 22 Oct 2019.
23. Diez-Ardanuy C, Greaves J, Munro KR, Tomkinson NC, Chamberlain LH. A cluster of palmitoylated cysteines are essential for aggregation of cysteine-string protein mutants that cause neuronal ceroid lipofuscinosis. *Sci Rep.* 2017;7:10.
24. Burgoyne RD, Morgan A. Cysteine string protein (CSP) and its role in preventing neurodegeneration. *Semin Cell Dev Biol.* 2015;40:153–9.
25. Gorenberg EL, Chandra SS. The role of co-chaperones in synaptic proteostasis and neurodegenerative disease. *Front Neurosci.* 2017;11:248.
26. Fogel BL. Genetic and genomic testing for neurologic disease in clinical practice. *Handb Clin Neurol.* 2018;147:11–22.

CLINICAL REPORT

Spinal muscular atrophy caused by a novel *Alu*-mediated deletion of exons 2a-5 in *SMN1* undetectable with routine genetic testing

Ivana Jedličková¹  | Anna Přistoupilová¹  | Lenka Nosková¹  | Filip Majer¹  |
 Viktor Stránecký¹  | Hana Hartmannová¹  | Kateřina Hodaňová¹  |
 Helena Trešlová¹  | Michaela Hýblová² | Peter Solár³  | Gabriel Minárik² |
 Mária Giertlová² | Stanislav Kmoch¹ 

¹Research Unit for Rare Diseases, Department of Pediatrics and Adolescent Medicine, First Faculty of Medicine, Charles University, Prague, Czech Republic

²Department of Clinical Genetics, Medirex A.S., Kosice, Slovakia

³Department of Medical Biology, Faculty of Medicine, P.J. Safarik University, Kosice, Slovakia

Correspondence

Ivana Jedličková, Research Unit for Rare Diseases, Department of Pediatrics and Adolescent Medicine, First Faculty of Medicine, Charles University, Ke Karlovu 455/2, 128 08 Prague, Czech Republic.
 Email: ivana.jedlickova@1f1.cuni.cz

Funding information

Research and Development for Innovations Operational Programme (RDIO) co-financed by European regional development fund and the state budget of the Czech Republic, Grant/Award Number: CZ.1.05/2.1.00/19.0400; Charles University, Grant/Award Number: PRVOUK-P24/LF1/3, SVV2016/260148 and UNCE 204064; Ministry of Education, Youth and Sports of the Czech Republic, Grant/Award Number: LQ1604 NPU II; Ministry of Health of the Czech Republic, Grant/Award Number: NV19-08-00137; The National Center for Medical Genomics, Grant/Award Number: LM2018132

Abstract

Background: Spinal muscular atrophy (SMA) is an inherited neuromuscular disease affecting 1 in 8,000 newborns. The majority of patients carry bi-allelic variants in the survival of motor neuron 1 gene (*SMN1*). *SMN1* is located in a duplicated region on chromosome 5q13 that contains *Alu* elements and is predisposed to genomic rearrangements.

Due to the genomic complexity of the *SMN* region and genetic heterogeneity, approximately 50% of SMA patients remain without genetic diagnosis that is a prerequisite for genetic treatments. In this work we describe the diagnostic odyssey of one SMA patient in whom routine diagnostics identified only a maternal heterozygous *SMN1*Δ(7–8) deletion.

Methods: We characterized *SMN* transcripts, assessed *SMN* protein content in peripheral blood mononuclear cells (PBMC), estimated *SMN* genes dosage, and mapped genomic rearrangement in the *SMN* region.

Results: We identified an *Alu*-mediated deletion encompassing exons 2a-5 of *SMN1* on the paternal allele and a complete deletion of *SMN1* on the maternal allele as the cause of SMA in this patient.

Conclusion: *Alu*-mediated rearrangements in *SMN1* can escape routine diagnostic testing. Parallel analysis of *SMN* gene dosage, *SMN* transcripts, and total *SMN* protein levels in PBMC can identify genomic rearrangements and should be considered in genetically undefined SMA cases.

KEYWORDS

Alu elements, *SMN1*, *SMN2*, spinal muscular atrophy

Ivana Jedličková and Anna Přistoupilová should be considered joint first author.

This is an open access article under the terms of the Creative Commons Attribution License, which permits use, distribution and reproduction in any medium, provided the original work is properly cited.

© 2020 The Authors. *Molecular Genetics & Genomic Medicine* published by Wiley Periodicals LLC

1 | INTRODUCTION

Spinal muscular atrophy (SMA) is an inherited neuromuscular disease characterized by progressive degeneration of alpha motor neurons in the spinal cord leading to muscle weakness and paralysis. SMA is the most prevalent monogenic cause of death in infancy (Glascock et al., 2018) with an incidence of ~1:8,000 in Caucasians and Asians and carrier frequency of ~1:50 (Verhaart et al., 2017). The severity of SMA can vary from early postnatal onset and muscular weakness with respiratory insufficiency to milder forms presenting during infancy or adolescence (Schorling et al., 2019). The majority of SMA patients carry bi-allelic variants in the survival of motor neuron 1 gene (*SMN1*, OMIM 600354) that localizes to a duplicated region on chromosome 5q13.

The survival of motor neuron 2 gene (*SMN2*, OMIM 601627) is a homologue of *SMN1*. Genetic investigations have revealed zero to six copies of *SMN2* that are located next to *SMN1* on 5q13 (Crawford et al., 2012). *SMN1* and *SMN2* (“*SMN* genes”) encode for the same SMN protein. However, expression of the SMN protein from *SMN2* is substantially lower than from *SMN1* due to a single nucleotide sequence difference at the sixth position of exon 7 in *SMN2* (hg38, chr5:70076526, T). This sequence difference alters splicing and results in the predominant production of an *SMN2* transcript that skips exon 7 (*SMN2Δ7*) and encodes for an unstable and less functional protein. *SMN2* is therefore unable to fully compensate the deficit of *SMN1*. However, SMN expression from *SMN2* may be increased in a gene dose-dependent manner (Crawford et al., 2012). This *SMN2* dose variance was suggested to have a compensatory effect on SMN expression and ameliorate the severity of SMA (Butchbach, 2016).

The *SMN* region on chromosome 5q13 is enriched for primate-specific nonautonomous retrotransposons belonging to a class of short interspersed elements (SINE)-repetitive DNA sequences called *Alu* elements. The *Alu* elements are about 280 base pairs long and are formed by two diverged dimers (Deininger, 2011). They are divided into subfamilies based on single nucleotide differences. The main *Alu* subfamilies are *AluJ*, *AluS*, and *AluY* (Kim, Cho, Han, & Lee, 2016) with the *AluY* being the evolutionarily youngest and *AluS* the most numerous. The youngest *Alu* subfamilies *AluS* and *AluY* increase the likelihood of genomic rearrangements that result in the formation of a new chimeric *Alu-Alu* element at the breakpoint junction.

Alu-mediated genomic rearrangements are a frequent cause of various human diseases (Song et al., 2018). Accordingly, 95% of genetically defined SMA patients have deletions of exons 7 and/or 8 of *SMN1* (*SMN1Δ7*, *SMN1Δ(7–8)*) that appear to be caused by *Alu*-mediated rearrangements (Ottesen, Seo, Singh, & Singh, 2017).

It is important to note that the term “deletion of *SMN1* exons 7 and/or 8” is commonly used to describe the results of

routinely performed multiplex ligation-dependent probe amplification (MLPA) assays, which are the current gold standard of SMA diagnostics (Mercuri et al., 2018). Deletions of these two particular exons can be detected by the MLPA assay, which is designed to target exclusively exons 7 and 8 and distinguishes *SMN1* and *SMN2* based on single nucleotide sequence differences. In reality, these deletions can extend beyond exons 7 and 8 and include the entire *SMN1*, then even extending further to include multigene deletions of the 5q13 region.

Other *Alu*-mediated genomic rearrangements in the *SMN* region identified in SMA patients lead to formation of *SMN1-SMN2* hybrid genes (van der Steege et al., 1996). Interestingly, *Alu*-mediated deletion of exons 4 to 6 with intact exons 7 and 8 has thus far been reported in just a single case (Wirth et al., 1999). Other *SMN1* variants identified in SMA patients include small intragenic deletions and missense variants. A full list of these variants can be found in the Human Gene Mutation Database records (Stenson et al., 2014).

Recently, non-5q-*SMN1* variants have been reported in SMA patients, including variants in *VRK1* (Renbaum et al., 2009), *EXOSC3* (Wan et al., 2012), *EXOSC8* (Boczonadi et al., 2014), and *SLC25A46* (Wan et al., 2016). Variants in these genes have been reclassified as a distinct syndrome pontocerebellar hypoplasia (OMIM 607596). Similarly, variants in *AGTPBP1* (Karakaya et al., 2019; Shashi et al., 2018) have also been reported to cause childhood-onset neurodegeneration with cerebellar atrophy (OMIM 618276), a different type of motor neuron disease.

Due to the complexity of the *SMN* 5q13 genomic region, approximately 50% of all SMA patients remain without a genetic diagnosis after routine genetic testing (Karakaya et al., 2018). The ability to identify the genetic cause of SMA is critically important for patients because only patients with bi-allelic *SMN1* variants are eligible for genetic therapies (Michelson et al., 2018). These potential treatments include Zolgensma and the antisense oligonucleotide treatment Spinraza. The precise identification of the causal variants in SMA patients is also important for genetic counseling in affected families.

In this work we describe the diagnostic odyssey for one SMA patient and her parents from Slovakia in whom the routine MLPA assay and subsequent direct sequencing of *SMN1* coding regions identified only a heterozygous, maternally inherited deletion of exons 7 and 8 in *SMN1*.

2 | MATERIALS AND METHODS

2.1 | Ethical compliance

The study was approved by the appropriate institutional review boards and the investigations were performed according to the Declaration of Helsinki principles. Parents provided informed consent.

2.2 | Clinical report

The patient was clinically diagnosed at the Children Teaching Hospital Košice, Slovakia. The infant was born by normal spontaneous delivery to a 31-year-old mother following a full-term pregnancy from the first gravidity and with no reported abortions; the postnatal adaptation of the infant was standard. The patient presented with global muscle hypotonia and hyporeflexia suggestive of SMA at the age of 1 month and showed markedly decreased mobility at the age of 3 months. Global respiratory failure required tracheostomy and mechanical ventilation from the age of 7 months. At the time of investigation, the patient was 2 years and 8 months old and ventilator dependent. She suffered from severe global weakness and hypotonia. Muscle atrophy predominantly affected the lower limbs. The patient could respond only with eye contact. There were no sensory deficits. Both parents were neurologically intact.

2.3 | MLPA, panel sequencing, and cytogenetic analyses

Genomic DNA (gDNA) was isolated from peripheral venous blood in the patient and her parents using standard protocol. The patient's karyotype was assessed by G-banding and comparative genomic hybridization (aCGH) was performed using Agilent SurePrint HD 4x44 platform at the Medirex Group, Slovakia. Genes associated with a set of neuromuscular disorders were analyzed using a custom SeqCap EZ kit (Roche) and Illumina sequencing at CMBGT in Brno, Czech Republic. The TruSight One Sequencing Panel (Illumina) was used for analysis of more than 4,800 genes associated with human diseases at Medirex. The presence of the deletion of exons 7 and 8 in *SMN* genes was assessed using the MLPA assay; SALSA MLPA P060 SMA Carrier probemix (MRC-Holland) at Genexpress. The coding regions of *SMN* genes were analyzed using paired-end sequencing of PCR amplicons on Illumina MiSeq (Illumina) at Alpha Medical.

2.4 | *SMN1* and *SMN2* mRNA/ cDNA analysis

Total RNA and cDNA were isolated and prepared from peripheral blood mononuclear cells (PBMC) using ProtoScript® II Reverse Transcriptase (NEB). Full-length *SMN1* and *SMN2* cDNAs were PCR amplified using primers SMN575_F (Sun et al., 2005) and SMN_541C1120_R (Lefebvre et al., 1995) (Table 1) amplifying together both *SMN* genes derived transcripts from the first coding exon to the last untranslated exon 8 (NM_000344.3). PCR products were analyzed

using the agarose gel electrophoresis, and Sanger sequenced using the version 3.1 Dye Terminator cycle sequencing kit (ThermoFisher Scientific) with electrophoresis on an ABI 3500XL Avant Genetic Analyzer (ThermoFisher Scientific).

2.5 | Western blot analysis of SMN protein

The quality and amount of the SMN protein were assessed in lysates of PBMC using Western blot analysis. PBMC were isolated using the Histopaque-1077 reagent (Sigma-Aldrich). The cell pellet was resuspended in 50 mM Tris pH 6.8, 50 mM DTT, 2% SDS, and Complete Protease Inhibitor Cocktail (Roche), sonicated using the Covaris S2 Ultrasonicator (Covaris), and denatured at 100°C for 10 min. The protein content in the supernatant was determined using an infrared spectrometer Direct Detect (Millipore) according to the manufacturer's protocol. Protein lysates equivalent to 22 µg of protein were reduced and denatured at 100°C for 10 min in a sample buffer with 1% beta-mercaptoethanol before SDS-PAGE electrophoresis. After protein transfer to the polyvinylidene fluoride (PVDF) membrane, the membrane was blocked by 5% skimmed milk and 0.1% Tween 20 in PBS for 1 hr at room temperature (RT). The SMN protein was visualized by incubation with mouse monoclonal SMN antibody (610646, BD Transductions) at 1:5,000 in 5% BSA and 0.1% Tween 20 in PBS over night at 4°C, followed by incubation with goat anti-mouse HRP (Pierce) at 1:10,000 in 0.1% Tween 20 in PBS for 60 min, and detection was performed by Clarity Western ECL Substrate (Bio-Rad). The actin protein was visualized by incubation with rabbit Actin antibody (A2103; Sigma-Aldrich) at 1:1,000 in 0.1% BSA and 0.1% Tween 20 in PBS for 1 hr at RT, followed by incubation with goat anti-rabbit HRP (Pierce) under conditions and using detection as described above. Relative quantification of the SMN protein was performed using GeneTools software (4.03.03.0, Syngene). SMN protein levels were normalized to actin; the experiment was performed in three technical replicates. The statistical significance was determined using one-way ANOVA test.

2.6 | Long-range PCR

Long-range PCR was performed using four primer pairs amplifying both *SMN* genes (NG_008691.1, NG_008728.1) in four overlapping PCR products (PCR1-PCR4, Table 1). The reactions were performed with TaKaRa LA PCR Kit Ver. 2.1 according to the manufacturer's protocol. PCR products were pair-end sequenced on Illumina HiSeq 2500 (Illumina). FASTQ files were aligned to the human reference genome hg19 using NovoAlign (V2.08.03) and all alignment locations

TABLE 1 Primers used for long-range PCR, qPCR, and *SMN* cDNAs amplification and *Alu* PCR

Primer ID	Primer sequence (5'–3')	Primers application
SMN1_1U	TTAAGGATCTGCCGCTTCC	Long-range PCR, PCR1 (<i>SMN1</i>)
SMN_1L	CCAAACCAGCCCACACATTG	
SMN_2U	CTACAGTAGCTGGGGACTGAGC	Long-range PCR, PCR2
SMN_2L	CATATGGAGGAAACCGGCCTAA	
SMN_3U	CACCATGCCCGGCCTAAAT	Long-range PCR, PCR3
SMN_3L	CAAGAGCACTGCATCTGGGT	
SMN_4U	AGCCAGGTCTAAAATTCAATGGC	Long-range PCR, PCR4
SMN_4L	TGGGCCAAAGGGCAAAAATAA	
SMN575_F	ATCCGCGGGTTTGCTATG	cDNA <i>SMN</i> exons 1–8
SMN_541C1120_R	CTACAACACCCTTCTCACAG	
SMN_i1_105_F	TCCCTATTAGCGCTCTCAGC	qPCR <i>SMN</i> region; I3
SMN_i1_182_R	CGGATCGACTTGATGCTGT	
SMN_ei3_7_F	ACAAAATGCTCAAGAGGTAAGGA	qPCR <i>SMN</i> region; E3I3
SMN_i3_96_R	TCGGTGGATCAAACCTGACAA	
SMN_i5e6_2_F	AAACAATATCTTTTCTGTCTCCAGAT	qPCR <i>SMN</i> region; I5E6
SMN_e6_797_R	GAAATTAACATACTTCCCAAAGCATC	
SMN_28867_F	TGTCCTGTGGTTGTAAGGAATC	qPCR <i>SMN</i> region; +1 kb
SMN_28961_R	CAGCAACTTTTGTCTGTCTTCTG	
Alu_259_wt_R	CCAGGCTGGAGTGCAGTGG	<i>Alu</i> PCR
Alu_259_4A_R	CCAGGCTGGAGTGCATATGG	<i>Alu</i> PCR
Alu_259_3C_R	CCAGGCTGGAGTGCAGCGG	<i>Alu</i> PCR
Alu_259_1A_R	CCAGGCTGGAGTGCAGCGA	<i>Alu</i> PCR
SMN_i5_979_R	AACGAGGACGAAAAGACAGC	<i>Alu</i> PCR
SMN_i5_821_R	ACAGCTCACATAGCATTTCG	<i>Alu</i> PCR sequencing
SMN_i1_10748_F	GGACTTGTCTCACTAATCCCTCAT	Family screening for <i>SMN(2a–5)</i> transcript
SMN_i5e6_1R	GGAGGTGGTGGGGGAATTATC	

were reported. Picard Tools (1.129) were used to convert SAM to BAM, remove duplicates, and add read groups. Local realignment around indels, base recalibration, and genotyping was performed with the Genome Analysis Toolkit, GATK (3.5) (McKenna et al., 2010). Variants were annotated by SnpEff (4.3t) (Cingolani et al., 2012) and GEMINI (0.20.2-dev) (Paila, Chapman, Kirchner, & Quinlan, 2013).

2.7 | Copy number analysis of *SMN* genes

The total number (sum) of *SMN* genes dosage was determined in the gDNA of the patient and her parents using the quantitative PCR (qPCR) analysis of four retrotransposon-free *SMN* genomic regions: (a) in intron 1 (I1), (b) in the exon 3–intron 3 junction (E3I3), (c) in the intron 5–exon 6 junction (I5E6), and (d) ~1 kb downstream from exon 8 (+1 kb) (Table 1). The qPCR was performed using the LightCycler® 480 System (Roche Applied Science). All of

the qPCR reactions were performed in triplicates in 10 μ l reactions with the following final concentrations of the reagents: 80 nM UPL probe, 300 nM primers, 1x Roche Probe Master Mix, and total 15 ng of genomic DNA per reaction. Sample quantitation cycle (cq) values were determined using the Second Derivative Maximum Method and normalized using the RNase P and albumin genes as a references. Relative quantification using the $2^{-\Delta\Delta CT}$ method (Livak & Schmittgen, 2001) was performed to determine the sum copy number. Unrelated healthy controls were used as control samples.

2.8 | Mapping of *SMN1* deletion breakpoint/junction by *Alu* PCR

The *Alu* PCR was performed as described previously by Majer et al. (2020). Briefly, based on the *SMN1* transcript analysis that identified deletion of exons 2a to exon 5 in

SMN1 cDNA, we anticipated that the deletion breakpoints must be located in adjacent introns 1 and 5. We identified in these regions sequences of *Alu* retrotransposons (Figure S1) and designed (a) a set of universal reverse primers targeting the terminal parts of the *Alus* in intron 1 (Alu_259_wt_R, Alu_259_4A_R, Alu_259_3C_R, Alu_259_1A_R) (Table 1, Figure S1), and (b) one *SMN1*-specific forward primer targeting from intron 5 toward intron 1 (SMN_i5_979_R, Table 1). We performed four separate PCR reactions (Figure S2) with the intron 5 *SMN1*-specific primer and one of the four *Alu* universal primers. Resulting PCR products of the four reactions were column isolated and Sanger sequenced using a gene-specific primer located in intron 5 *Alu* preceding region (SMN_i5_821_R) (Table 1). The Sanger sequencing was performed as described above.

The deletion-spanning PCR method for testing of family members for the $\Delta 2a-5$ deletion was performed using primers annealing to the intron 1 (SMN_i1_10748_F) and exon 6 of *SMN1* (SMN_i5e6_1R, Table 1). Resulting PCR products were column isolated and Sanger sequenced as described above.

3 | RESULTS

3.1 | Routine genetic testing in the patient identified only heterozygous, maternally inherited deletion of exons 7 and 8 in *SMN1*

To establish the diagnosis, MLPA analysis was performed and revealed a deletion of *SMN1* exons 7 and 8 and two copies of *SMN2* exons 7 and 8. Heterozygous deletion of *SMN1* exons 7 and 8 was also found in the patient's mother, who also carried only one copy of *SMN2* exons 7 and 8. The father carried two copies of exons 7 and 8 of both *SMN* genes (Table 2).

Subsequent targeted sequencing of the coding regions of *SMN* genes in the patient and parents did not reveal any further pathogenic variants that would explain the SMA phenotype. To search for other potential disease-causing variants, karyotype assessment and array-based comparative genomic hybridization assay (aCGH) were performed but no gross chromosomal abnormalities were detected. The panel sequencing of genes associated with a set of

neuromuscular disorders and the TruSight One Sequencing Panel did not reveal any definitive or likely pathogenic variants related to the phenotype. Due to inconclusive results of genetic testing, the patient was referred to the Research Unit for Rare Diseases of the First Faculty of Medicine, Charles University in Prague, and included in the "Undiagnosed Disease Program" that aims to identify genetic diagnosis in cases of rare genetic diseases with negative results of genetic and genomic analyses.

Before looking for other genetic causes, the primary focus was to further analyze the *SMN* genomic region in this patient whose clinical phenotype was highly suggestive of SMA.

3.2 | Direct sequencing of *SMN* cDNAs revealed an absence of a full-length *SMN1* transcript in the patient

To study the *SMN1* transcript we performed reverse transcription polymerase chain reaction (RT-PCR) and amplified the full-length *SMN* cDNAs from PBMC of the patient, both parents and controls. Using the agarose gel electrophoresis, we observed in the patient and her father an abnormal PCR product of ~600 bp that was not present in mother and controls (Figure 1a). Subsequent Sanger sequencing of the gel isolated PCR products revealed the presence of the full-length *SMN1* and *SMN2* cDNA in the mother, father, and control. In the patient, only the full-length *SMN2* cDNA was present and the full-length *SMN1* cDNA was lacking. The abnormal shorter cDNA of ~600 base pairs that was detected in the patient and father was, based on the presence of two *SMN1*-specific sequence variants in exons 7 and 8, identified as a *SMN1* that was lacking exon 2a to exon 5 ($\Delta 2a-5$) (Figure 1a).

3.3 | Western blot analysis confirmed decreased amount of SMN protein in PBMC

To analyze the effect of identified mRNA changes on the protein quality and abundance, we immunodetected and quantified SMN protein in PBMC lysates from the patient, her parents, and a control. In all samples we detected only one immune-reactive protein at ~40 kDa, corresponding to the predicted molecular weight of full-length SMN (Figure 1b). The protein at the length of ~10 kDa corresponding to a predicted molecular weight of the deleted SMN($\Delta 2a-5$) was not detected probably due to its altered immunogenicity or reduced protein stability. Compared with controls, the amount of SMN normalized to actin was reduced to 10% in the patient, 27% in the mother, and 41% in the father (Figure 1c).

TABLE 2 Results of routine MLPA analysis

	<i>SMN1</i>		<i>SMN2</i>	
	Exon 7	Exon 8	Exon 7	Exon 8
Patient	1	1	2	2
Mother	1	1	1	1
Father	2	2	2	2

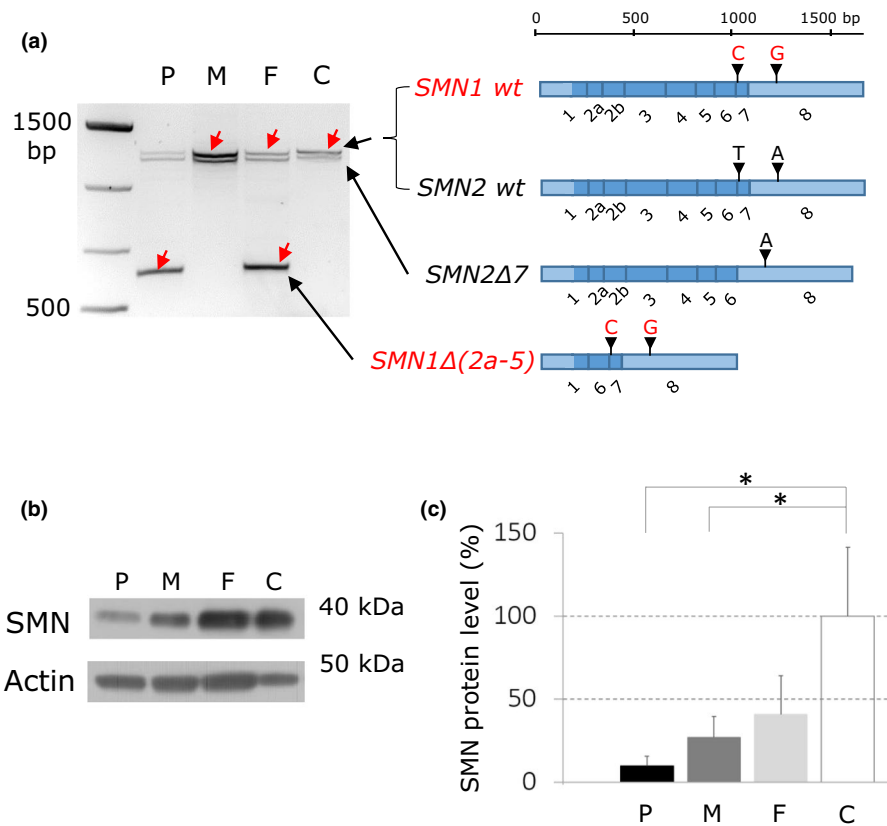
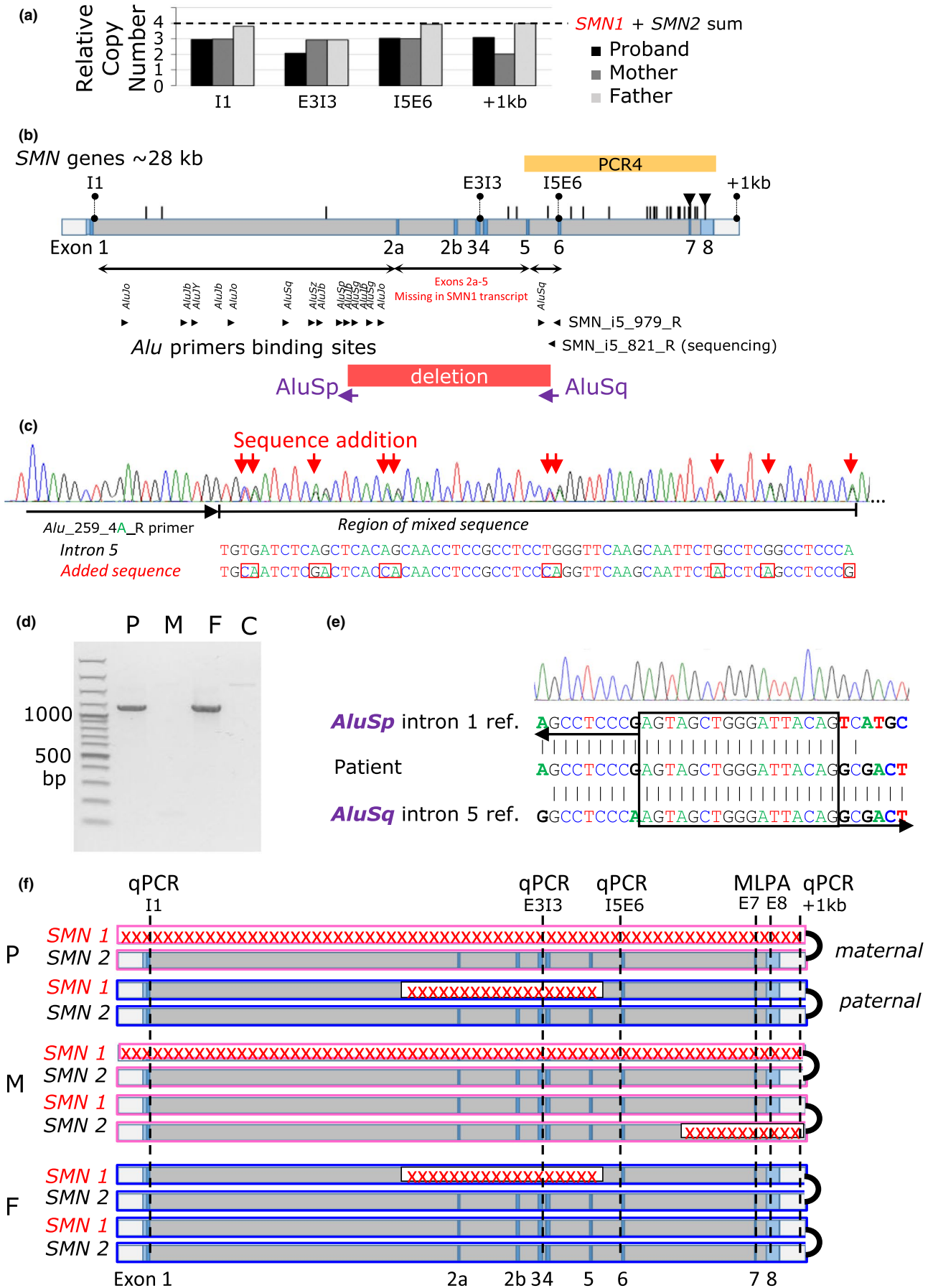


FIGURE 1 *SMN1* transcript and SMN protein analysis. (a) Agarose gel electrophoresis profiles of RT-PCR products amplified from total RNA isolated from PMBC of the patient (P), her mother (M), father (F), and control (C) showing presence of the abnormal RT-PCR product of ~600 base pairs in the patient and her father. Identities of individual RT-PCR products revealed by Sanger sequencing are shown on the right. (b) Western blot analysis of total PBMC homogenates. Detection with anti-SMN and anti-actin antibodies showed presence of immune-reactive proteins of molecular weights of ~40 and 50 kDa corresponding to predicted molecular weight of the SMN and actin, respectively. (c) The graph shows the relative amounts of SMN normalized to actin and decrease in SMN content in the patient (P), her mother (M), and father (F) compare with control (C). * $p < .05$

FIGURE 2 Identification of *SMN1* variants. (a) qPCR analysis of four retrotransposon-free *SMN* genomic regions in the intron 1 (I1), in the exon 3–intron 3 junction (E3I3), in the intron 5–exon 6 junction (I5E6), and ~1 kb downstream from exon 8 (+1 kb). Compared with four copies of *SMN* genes that are present in controls, we found that the patient has three copies at the I1, I5E6, and +1 kb loci and two copies at the E3I3 loci. The mother has three copies through the I1 to I5E6 loci and two copies at the +1 kb loci. The father has three copies only at the I5E6 loci. (b) Schematic representation of *SMN1/2* exon (E)/intron (I) structure. Positions of sequence differences between *SMN1* and *SMN2* are represented by black vertical bars. The black triangles denote sequence-specific variants in exons 7, 8 targeted by MLPA probes in routine testing. Locations of *Alus* in the breakpoint candidate regions in the intron 1 and 5, including the causal *AluSp* in the intron 1 and *AluSq* in the intron 5 indicated by vertical text, and primers binding sites for *Alu* PCR indicated by black arrowheads are shown below the scheme of the *SMN* structure. Position of the PCR4 spanning exons 5–8 that showed absence of *SMN1* sequence-specific variants indicating disruption of both *SMN1* alleles in the patient is represented by yellow box. Range of the paternal deletion of exons 2a–5 is represented by red box. (c) DNA sequence trace of the *Alu* PCR, *Alu_259_4A*, showing a double sequence caused by presence of *AluSq* wt in intron 5 together with a sequence originating from the intron 1 *AluSp*. Red arrows indicate the addition of *AluSp*-specific sequence in an *Alu* PCR product. (d) PCR genotyping of the *SMN1Δ(2a-5)* variant showed presence of the deletion-spanning amplification product in the patient (P) and father (F), but not in mother (M) and control (C). (e) DNA sequence trace of the breakpoint junction-specific PCR and detail of the $\Delta 2a-5$ breakpoint junction show the new *Alu-Alu* chimeric element originating from the recombination between the *AluSp* in the intron 1 and *AluSq* in the intron 5. A breakpoint microhomology of the *AluSp* and *AluSq* is marked with a black box. (f) Schematic representation of *SMN1* and *SMN2* in the family members. Pink-marked boxes represent maternal alleles (M) and blue boxes paternal alleles (F). The red crosses denote identified deletions and the dashed vertical lines denote loci of the qPCR (I1, E3I3, I5E6, and +1 kb) and MLPA (exon 7–E7, exon 8–E8) probes used for deletion mapping. The black junctions on the box terminals indicate a cis configuration of *SMN1* and *SMN2* alleles. The model shows (a) a whole deletion of one *SMN1* allele in the patient (P) inherited from her mother and detected by the combination of the qPCR and MLPA; (b) a deletion of the second *SMN1* allele in the patient inherited from her father and detected by the E3I3 qPCR and transcript analysis (Figure 1a); and (c) deletion of one copy of one *SMN2* allele in the mother detected by the MLPA and the +1 kb qPCR



3.4 | *SMN1* and *SMN2* gDNA copy number analyses suggested the presence of the intragenic *SMN1* deletion in the patient and father and whole-gene *SMN1* deletion in the patient and her mother

To assess *SMN* gene dosage, we performed qPCR analysis of four retrotransposon-free *SMN* genomic regions: (a) in intron 1 (I1), (b) in the exon 3–intron 3 junction (E3I3), (c) in the intron 5–exon 6 junction (I5E6), and (d) ~1 kb downstream from exon 8 (+1 kb). Compared with four copies of *SMN* genes that are normally present in each of four tested loci in controls, we found that the patient has three copies at the I1, I5E6, and +1 kb loci and two copies at the E3I3 loci. The mother has three copies through the I1 to I5E6 loci and two copies at the +1 kb loci. The father has three copies only at the I5E6 loci (Figure 2a). Together with the MLPA assay findings (Table 2), this analysis suggested that the patient had deletion of the whole *SMN1* on the maternal allele (NC_000005.9:g.(?_70221078)_70249850_?)del, where the genomic coordinates denote the central position of the qPCR probes targeting the I1 and +1 kb genomic loci, and a deletion encompassing $\Delta 2a-5$ exons of *SMN1* on the paternal allele.

3.5 | Sequencing of long-range gDNA PCR products spanning *SMN* genomic sequence indicated bi-allelic deletion of the *SMN1* in the patient

To identify the variant causing the deletion of *SMN1* exons 2a-5 in the patient's and father's cDNA, we PCR amplified the genomic DNA and Illumina sequenced four overlapping long-range amplicons (PCR1–PCR4) spanning exons 1–8 of *SMN1* and *SMN2*. Using specific single nucleotide sequence differences that distinguish the *SMN* genes, we found that in the patient amplicon PCR4, spanning intron 6, exon 7, intron 7, and exon 8 (Figure 2b), had been amplified exclusively from *SMN2*. These findings indicated that *SMN1* gene must be disrupted on both alleles in the patient.

3.6 | *SMN1* deletion breakpoint/junction mapping revealed paternal *Alu*-mediated deletion

To identify the exact nature of the variant on the paternal allele, we considered the *Alu*-mediated rearrangement of *SMN1* as the most likely mechanism. Using computer analysis we identified in the candidate breakpoint region of intron 1 a set of 21 *Alus* (Figure 2b); in the candidate region of intron 5 we identified only one *AluSq* (Figure 2b). We considered *AluSq* to be a candidate breakpoint start site and anticipated recombination

between the *AluSq* and one of the *Alus* located in intron 1 resulting in the formation of a new chimeric *Alu*. With this assumption we performed four PCR reactions using always one of the universal *Alu* primers and the *SMN1* intron 5–specific primer flanking the *AluSq*. Sanger sequencing of obtained PCR products revealed that two of them contained both the wild-type (*wt*) *AluSq* sequence of intron 5 and the sequence originating from a new chimeric *Alu* resulting from the rearrangement with *AluSp* element originating from the intron 1 (Figure 2c; Figure S2).

Using this sequence we designed and performed a deletion-spanning PCR allowing for genotyping of the $\Delta 2a-5$ deletion. The deletion-spanning PCR product was obtained from DNA of the patient and her father, but not from the mother and control (Figure 2d). Sanger sequencing of this PCR product (Figure 2e) defined the new *Alu*-mediated *SMN1* deletion ranging 8,978 base pairs as NC_000005.9:g.70232118-70241095del; NM_000344.3:c.82-2548_723+515del.

3.7 | Genetic analysis of the *SMN* region correlates with the variance in *SMN* expression in PBMC

In summary, the genetic analysis (Figure 2f) established that the patient is a compound heterozygote for the ~9 kbp deletion in *SMN1* that she inherited from her father and the deletion of the entire *SMN1* that she inherited from her mother. Maternal and paternal *SMN2* alleles were intact. This genotype correlates with the very low (10% of controls) *SMN* content in PBMC that must be expressed exclusively from *SMN2* (Figure 2b,c). In addition to the deletion of the entire *SMN1*, the mother also has a deletion of the terminal part of *SMN2*. This correlates with reduced (27% of controls) *SMN* content in PBMC compared with the father (41% of controls), who has only the ~9 kbp deletion on one of the *SMN1* alleles and both *SMN2* alleles intact.

4 | DISCUSSION

Spinal muscular atrophy is devastating inherited neuromuscular disease resulting from variants of *SMN1* and deficiency of the survival motor neuron protein (SMN). Several clinical or experimental therapies for SMA augmenting levels of SMN are currently available or in development (Groen, Talbot, & Gillingwater, 2018). The treatment is provided only to individuals with an established genetic diagnosis. Despite great progress in genetic diagnostic methods, approximately half of the patients suspected to have SMA still remain without a genetic diagnosis after routine genetic testing (Karakaya et al., 2018). This unsatisfactory situation is due to the complexity of the *SMN* genomic region and lack of methods allowing routine identification of individual genomic rearrangements.

In this work, we describe the diagnostic odyssey for one SMA patient in whom routine diagnostic procedures identified only a heterozygous, maternally inherited deletion of exons 7 and 8 in *SMN1*. *SMN* is ubiquitously expressed and detectable in PBMC (Sumner et al., 2006). To identify the other *SMN1* variant in this case, we obtained PBMC from the patient and his parents. In this material we successively assessed *SMN* transcripts, *SMN* protein content, *SMN* genes dosage, and *SMN* genomic sequence. Using this approach we found in this case that SMA was caused by a novel *Alu*-mediated deletion encompassing exons 2a to exon 5 ($\Delta 2a-5$) of *SMN1* on the paternal allele and by deletion of whole *SMN1* on the maternal allele.

The ($\Delta 2a-5$) variant of *SMN1* escaped detection by the routine MLPA assay that targets only exons 7 and 8. To the best of our knowledge, this is only the second reported *Alu*-mediated deletion in *SMN1* that does not encompass the exons 7 and 8 (Wirth et al., 1999).

Our work suggests that other *Alu*-mediated rearrangements in the *SMN* region that escape detection with routine genetic testing may be more common and should be considered in SMA cases who remain without a genetic diagnosis after standard genetic testing.

We demonstrate that in these cases measurement of SMA protein in PBMC may successfully identify patients with SMA in whom a genetic diagnosis cannot be made. These individuals can then undergo further testing, including *SMN* gene dosage, full characterization of *SMN* transcripts, and precise characterization of the eventual genomic rearrangements. All these parameters are critical for targeted genotyping and eventually for prenatal or preconception analysis in affected families and therapeutic eligibility for affected individuals. We are interested to study other similar cases and can provide the genetic testing and biochemical analyses described here. Please contact ivana.jedlickova@lf1.cuni.cz.

ACKNOWLEDGMENTS

This work was supported by Ministry of Health of the Czech Republic, grant nr. NV19-08-137. Institutional support was provided by Charles University institutional programs PRVOUK-P24/LF1/3, UNCE 204064, and SVV2016/260148, by the project LQ1604 NPU II from the Ministry of Education, Youth and Sports of the Czech Republic. We thank The National Center for Medical Genomics (LM2018132) for their instrumental and technical support with the WES analyses. Instrumental support was provided by grant CZ.1.05/2.1.00/19.0400 from the Research and Development for Innovations Operational Programme (RDOP) cofinanced by European regional development fund and the state budget of the Czech Republic.











CONFLICT OF INTEREST

All authors have no conflict of interest to declare.

AUTHOR CONTRIBUTIONS

IJ, AP, LN, FM, GM, MG, and SK were involved in writing of the manuscript and revised the manuscript. IJ, LN, FM, HH, KHo, HT, KHý, PS, and MG performed the laboratory experiments and interpreted the data. AP, VS, and GM performed bioinformatic studies. MG ascertained the patient and provided the clinical evaluation of the patient. IJ, MG, and SK coordinated the study.

ORCID

Ivana Jedličková  <https://orcid.org/0000-0002-3362-0834>
 Anna Přistoupilová  <https://orcid.org/0000-0003-0047-9405>
 Lenka Nosková  <https://orcid.org/0000-0001-7011-4327>
 Filip Majer  <https://orcid.org/0000-0002-3549-6312>
 Viktor Stránecký  <https://orcid.org/0000-0002-2599-6479>
 Hana Hartmannová  <https://orcid.org/0000-0001-7787-832X>
 Kateřina Hodaňová  <https://orcid.org/0000-0001-9172-9945>
 Helena Trešlová  <https://orcid.org/0000-0003-0180-1179>
 Peter Solár  <https://orcid.org/0000-0002-1287-2979>
 Stanislav Kmoch  <https://orcid.org/0000-0002-6239-707X>

REFERENCES

- Boczonadi, V., Müller, J. S., Pyle, A., Munkley, J., Dor, T., Quartararo, J., ... Horvath, R. (2014). EXOSC8 mutations alter mRNA metabolism and cause hypomyelination with spinal muscular atrophy and cerebellar hypoplasia. *Nature Communications*, 5, 4287. <https://doi.org/10.1038/ncomms5287>
- Butchbach, M. E. (2016). Copy number variations in the survival motor neuron genes: Implications for spinal muscular atrophy and other neurodegenerative diseases. *Frontiers in Molecular Biosciences*, 3, 7. <https://doi.org/10.3389/fmolb.2016.00007>
- Cingolani, P., Platts, A., Wang, L. L., Coon, M., Nguyen, T., Wang, L., ... Ruden, D. M. (2012). A program for annotating and predicting the effects of single nucleotide polymorphisms, SnpEff: SNPs in the genome of *Drosophila melanogaster* strain w1118; iso-2; iso-3. *Fly (Austin)*, 6(2), 80–92. <https://doi.org/10.4161/fly.19695>
- Crawford, T. O., Paushkin, S. V., Kobayashi, D. T., Forrest, S. J., Joyce, C. L., Finkel, R. S., ... Chen, K. S. (2012). Evaluation of *SMN* protein, transcript, and copy number in the biomarkers for spinal muscular atrophy (BforSMA) clinical study. *PLoS ONE*, 7(4), e33572. <https://doi.org/10.1371/journal.pone.0033572>
- Deininger, P. (2011). *Alu* elements: Know the SINEs. *Genome Biology*, 12(12), 236. <https://doi.org/10.1186/gb-2011-12-12-236>
- Gluscock, J., Sampson, J., Haidet-Phillips, A., Connolly, A., Darras, B., Day, J., ... Jarecki, J. (2018). Treatment algorithm for infants diagnosed with spinal muscular atrophy through newborn screening. *Journal of Neuromuscular Diseases*, 5(2), 145–158. <https://doi.org/10.3233/JND-180304>
- Groen, E. J. N., Talbot, K., & Gillingwater, T. H. (2018). Advances in therapy for spinal muscular atrophy: Promises and challenges. *Nature Reviews Neurology*, 14(4), 214–224. <https://doi.org/10.1038/nrneuro.2018.4>
- Karakaya, M., Paketci, C., Altmueller, J., Thiele, H., Hoelker, I., Yis, U., & Wirth, B. (2019). Biallelic variant in *AGTPBP1* causes infantile lower motor neuron degeneration and cerebellar atrophy. *American Journal of Medical Genetics. Part A*, <https://doi.org/10.1002/ajmg.a.61198>


- Karakaya, M., Storbeck, M., Strathmann, E. A., Delle Vedove, A., Hölker, I., Altmueller, J., ... Wirth, B. (2018). Targeted sequencing with expanded gene profile enables high diagnostic yield in non-5q-spinal muscular atrophies. *Human Mutation*, *39*(9), 1284–1298. <https://doi.org/10.1002/humu.23560>
- Kim, S., Cho, C. S., Han, K., & Lee, J. (2016). Structural variation of Alu element and human disease. *Genomics Information*, *14*(3), 70–77. <https://doi.org/10.5808/GI.2016.14.3.70>
- Lefebvre, S., Bürglen, L., Reboullet, S., Clermont, O., Burlet, P., Viollet, L., ... Melki, J. (1995). Identification and characterization of a spinal muscular atrophy-determining gene. *Cell*, *80*(1), 155–165. [https://doi.org/10.1016/0092-8674\(95\)90460-3](https://doi.org/10.1016/0092-8674(95)90460-3)
- Livak, K. J., Schmittgen, T. D. (2001). Analysis of relative gene expression data using real-time quantitative PCR and the 2(-Delta Delta C(T)) Method. *Methods*, *25*(4), 402–408. <https://doi.org/10.1006/meth.2001.1262>
- Majer F., Kousal B., Dusek P., Piherova L., Reboun M., Mihalova R., ... Sikora J. (2020). Alu-mediated Xq24 deletion encompassing CUL4B, LAMP2, ATP1B4, TMEM255A, and ZBTB33 genes causes Danon disease in a female patient. *American Journal of Medical Genetics Part A*, *182*(1), 219–223.
- McKenna, A., Hanna, M., Banks, E., Sivachenko, A., Cibulskis, K., Kernytsky, A., ... DePristo, M. A. (2010). The genome analysis toolkit: A MapReduce framework for analyzing next-generation DNA sequencing data. *Genome Research*, *20*(9), 1297–1303. <https://doi.org/10.1101/gr.107524.110>
- Mercuri, E., Finkel, R. S., Muntoni, F., Wirth, B., Montes, J., Main, M., ... Szlagatys-Sidorkiewicz, A. (2018). Diagnosis and management of spinal muscular atrophy: Part 1: Recommendations for diagnosis, rehabilitation, orthopedic and nutritional care. *Neuromuscular Disorders*, *28*(2), 103–115. <https://doi.org/10.1016/j.nmd.2017.11.005>
- Michelson, D., Ciafaloni, E., Ashwal, S., Lewis, E., Narayanaswami, P., Oskoui, M., & Armstrong, M. J. (2018). Evidence in focus: Nusinersen use in spinal muscular atrophy: Report of the Guideline Development, Dissemination, and Implementation Subcommittee of the American Academy of Neurology. *Neurology*, *91*(20), 923–933. <https://doi.org/10.1212/WNL.0000000000006502>
- Ottesen, E. W., Seo, J., Singh, N. N., & Singh, R. N. (2017). A multi-layered control of the human survival motor neuron gene expression by Alu elements. *Frontiers in Microbiology*, *8*, 2252. <https://doi.org/10.3389/fmicb.2017.02252>
- Paila, U., Chapman, B. A., Kirchner, R., & Quinlan, A. R. (2013). GEMINI: Integrative exploration of genetic variation and genome annotations. *PLoS Computational Biology*, *9*(7), e1003153. <https://doi.org/10.1371/journal.pcbi.1003153>
- Renbaum, P., Kellerman, E., Jaron, R., Geiger, D., Segel, R., Lee, M., ... Levy-Lahad, E. (2009). Spinal muscular atrophy with pontocerebellar hypoplasia is caused by a mutation in the VRK1 gene. *American Journal of Human Genetics*, *85*(2), 281–289. <https://doi.org/10.1016/j.ajhg.2009.07.006>
- Schorling, D. C., Becker, J., Pechmann, A., Langer, T., Wirth, B., & Kirchner, J. (2019). Discrepancy in redetermination of SMN2 copy numbers in children with SMA. *Neurology*, <https://doi.org/10.1212/WNL.0000000000007836>
- Shashi, V., Magiera, M. M., Klein, D., Zaki, M., Schoch, K., Rudnik-Schöneborn, S., ... Senderek, J. (2018). Loss of tubulin deglutamylase CCP1 causes infantile-onset neurodegeneration. *EMBO Journal*, *37*(23), <https://doi.org/10.15252/embj.2018100540>
- Song, X., Beck, C. R., Du, R., Campbell, I. M., Coban-Akdemir, Z., Gu, S., ... Lupski, J. R. (2018). Predicting human genes susceptible to genomic instability associated with Alu/Alu-mediated rearrangements. *Genome Research*, *28*(8), 1228–1242. <https://doi.org/10.1101/gr.229401.117>
- Stenson, P. D., Mort, M., Ball, E. V., Shaw, K., Phillips, A., & Cooper, D. N. (2014). The human gene mutation database: Building a comprehensive mutation repository for clinical and molecular genetics, diagnostic testing and personalized genomic medicine. *Human Genetics*, *133*(1), 1–9. <https://doi.org/10.1007/s00439-013-1358-4>
- Sumner, C. J., Kolb, S. J., Harmison, G. G., Jeffries, N. O., Schadt, K., Finkel, R. S., ... Fischbeck, K. H. (2006). SMN mRNA and protein levels in peripheral blood: Biomarkers for SMA clinical trials. *Neurology*, *66*(7), 1067–1073. <https://doi.org/10.1212/01.wnl.0000201929.56928.13>
- Sun, Y., Grimmler, M., Schwarzer, V., Schoenen, F., Fischer, U., & Wirth, B. (2005). Molecular and functional analysis of intragenic SMN1 mutations in patients with spinal muscular atrophy. *Human Mutation*, *25*(1), 64–71. <https://doi.org/10.1002/humu.20111>
- van der Steege, G., Grootsholten, P. M., Cobben, J. M., Zappata, S., Scheffer, H., den Dunnen, J. T., ... Buys, C. H. (1996). Apparent gene conversions involving the SMN gene in the region of the spinal muscular atrophy locus on chromosome 5. *American Journal of Human Genetics*, *59*(4), 834–838. Retrieved from <http://www.ncbi.nlm.nih.gov/pubmed/8808598>
- Verhaart, I. E. C., Robertson, A., Wilson, I. J., Aartsma-Rus, A., Cameron, S., Jones, C. C., ... Lochmüller, H. (2017). Prevalence, incidence and carrier frequency of 5q-linked spinal muscular atrophy - a literature review. *Orphanet Journal of Rare Diseases*, *12*(1), 124. <https://doi.org/10.1186/s13023-017-0671-8>
- Wan, J., Steffen, J., Yourshaw, M., Mamsa, H., Andersen, E., Rudnik-Schöneborn, S., ... Jen, J. C. (2016). Loss of function of SLC25A46 causes lethal congenital pontocerebellar hypoplasia. *Brain*, *139*(11), 2877–2890. <https://doi.org/10.1093/brain/aww212>
- Wan, J., Yourshaw, M., Mamsa, H., Rudnik-Schöneborn, S., Menezes, M. P., Hong, J. E., ... Jen, J. C. (2012). Mutations in the RNA exosome component gene EXOSC3 cause pontocerebellar hypoplasia and spinal motor neuron degeneration. *Nature Genetics*, *44*(6), 704–708. <https://doi.org/10.1038/ng.2254>
- Wirth, B., Herz, M., Wetter, A., Moskau, S., Hahnen, E., Rudnik-Schöneborn, S., ... Zerres, K. (1999). Quantitative analysis of survival motor neuron copies: Identification of subtle SMN1 mutations in patients with spinal muscular atrophy, genotype-phenotype correlation, and implications for genetic counseling. *American Journal of Human Genetics*, *64*(5), 1340–1356. <https://doi.org/10.1086/302369>

SUPPORTING INFORMATION

Additional supporting information may be found online in the Supporting Information section.

How to cite this article: Jedličková I, Přistoupilová A, Nosková L, et al. Spinal muscular atrophy caused by a novel *Alu*-mediated deletion of exons 2a-5 in *SMN1* undetectable with routine genetic testing. *Mol Genet Genomic Med*. 2020;8:e1238. <https://doi.org/10.1002/mgg3.1238>

NOTCH2NLC CGG Repeats Are Not Expanded and Skin Biopsy Was Negative in an Infantile Patient With Neuronal Intranuclear Inclusion Disease

Ivana Jedlickova, MSc, Anna Pristoupilova, MSc, Helena Hulkova, MD, PhD, Alena Vrbacka, PhD, Viktor Stranecky, PhD, Eva Hrubá, MD, Pavel Jesina, MD, PhD, Tomas Honzik, MD, PhD, Ivan Hrdlicka, PhD, Jiri Fremuth, MD, PhD, Kristyna Pivovarcikova, MD, PhD, Ibrahim Bitar, PhD, Radoslav Matej, MD, PhD, Stanislav Kmoch, PhD, and Jakub Sikora , MD, PhD

Abstract

Neuronal intranuclear inclusion disease (NIID) is a progressive neurodegenerative disorder categorized into 3 phenotypic variants: infantile, juvenile, and adult. Four recent reports have linked NIID to CGG expansions in the *NOTCH2NLC* gene in adult NIID (aNIID) and several juvenile patients. Infantile NIID (iNIID) is an extremely rare neuropediatric condition. We present a 7-year-old male patient with severe progressive neurodegenerative disease that included cerebellar symptoms with cerebellar atrophy on brain MRI, psychomotor developmental regression, pseudobulbar syndrome, and polyneuropathy. The diagnosis of iNIID was established through a postmortem neuropathology work-up. We performed long-read sequencing of the critical *NOTCH2NLC* repeat motif and found no expansion in the patient. We also re-evaluated an antemortem skin biopsy that was collected when the patient was 2 years and 8 months

old and did not identify the intranuclear inclusions. In our report, we highlight that the 2 methods (skin biopsy and CGG expansion testing in *NOTCH2NLC*) used to identify aNIID patients may provide negative results in iNIID patients.

Key Words: Cerebellum, Infantile neuronal intranuclear inclusion disease, Neuropathology, *NOTCH2NLC*, Trinucleotide repeat expansions.

INTRODUCTION

Neuronal intranuclear inclusion disease (NIID) is a progressive neurodegenerative disorder that is categorized into 3 variants (infantile, juvenile, and adult) based on the age of onset, duration, clinical neurological symptoms, and brain MRI findings (1, 2). Intranuclear eosinophilic inclusions with typical immunohistochemical (IHC) and ultrastructural profiles are the cellular characteristic of NIID. These inclusions are found not only in neurons, but also in other cell types including nonneuronal tissues. The number of adult NIID (aNIID) patients has grown lately due to efficient antemortem diagnostics based on skin biopsy assessment (1, 3).

Infantile NIID (iNIID) is an extremely rare neuropediatric disease that has multiple clinical and (neuro)pathological aspects consistently distinct from aNIID. Only 7 iNIID patients have been reported to date (4–6). Six of these patients presented with a very similar clinical phenotype characterized by an abrupt mental and motor developmental regression before the age of 4 years and death ensued by 9 years of age, at the latest. Though a complex disease, cerebellar symptoms and hypotonia seem to prevail in iNIID (4–6). All reported iNIID patients were diagnosed postmortem by identification of neuronal intranuclear inclusions in the nervous system. Cerebellar atrophy is an additional iNIID characteristic. Antemortem skin biopsy findings were reported in just one iNIID patient by Pilson et al (6). However, the biopsied tissue lacked the intranuclear inclusions seen in the skin samples of adult NIID patients. Based on these observations, the latter authors

Department of Pediatrics and Adolescent Medicine, Research Unit for Rare Diseases (IJ, AP, HH, AV, VS, EH, PJ, TH, SK, JS); Institute of Pathology (HH, RM, JS); Institute of Biology and Medical Genetics (IH), First Faculty of Medicine, Charles University and General University Hospital, Prague, Czech Republic; Department of Pediatrics (JF); Sikl's Department of Pathology (KP); Biomedical Center (IB), Faculty of Medicine in Pilsen, Charles University, Czech Republic; Department of Pathology and Molecular Medicine (RM), Third Faculty of Medicine, Charles University and Thomayer Hospital, Prague, Czech Republic

Send correspondence to: Jakub Sikora, MD, PhD, Department of Pediatrics and Adolescent Medicine, Research Unit for Rare Diseases, First Faculty of Medicine, Charles University and General University Hospital, Ke Karlovu 2, 128 00 Prague 2, Czech Republic; E-mail: jakub.sikora@lf1.cuni.cz

Ivana Jedlickova and Anna Pristoupilova contributed equally to this work. This study was supported by Ministry of Health of the Czech Republic (grant NV19-08-137) and OPPK (grant CZ.2.16/3.1.00/24509). Institutional support was provided by Charles University institutional programs UNCE 204064, SVV2016/260148, and PROGRES Q26 and Q39, and RVO VFN64165 from the Ministry of Health. We thank The National Center for Medical Genomics (LM2018132) for their instrumental and technical support with the NGS analyses.

The authors have no duality or conflicts of interest to declare.

Supplementary Data can be found at academic.oup.com/jnen.

claimed that further studies are warranted to establish the sensitivity of skin biopsy testing in NIID.

Four parallel studies ([7–10]; all published from June to August 2019) in NIID families and sporadic NIID patients have linked NIID to expansions of GGC (7, 9, 10) (or alternatively CGG [8]) repeat in the *NOTCH2NLC* gene. Of particular importance, patient cohorts tested by these 4 research groups (>130 patients were analyzed in total) were comprised adult (and several juvenile) NIID patients. Ishiura et al noted the possibility of genetic heterogeneity of NIID as their NIID cohort included 2 patients who did not have CGG expansions in *NOTCH2NLC* (8). None of the 4 reports (7–10), however, presented molecular genetic analyses of samples from iNIID patient(s).

We recently established the diagnosis of iNIID in a 7-year-old boy (eighth documented patient overall) through postmortem tissue analyses. In our report, we summarize the neuropathology findings, confirm negative results of the antemortem skin biopsy and demonstrate normal number of *NOTCH2NLC* CGG repeats in the patient.

MATERIALS AND METHODS

The study was approved by the Ethics Committee of the authors' home institution. Informed consent for presentation of the results was obtained from all participants.

Histopathology, Immunohistochemistry, Electron Microscopy, and Image Acquisition

Formalin-fixed brain and spinal cord were sectioned (Supplementary Data Table S1) and embedded into paraffin (FFPE). Liver, spleen, lungs, heart, and kidneys were processed identically. All FFPE tissue blocks from the brain, spinal cord, and visceral organs were cut into 2–5- μ m-thick sections and stained routinely by hematoxylin and eosin; unstained sections were mounted for autofluorescence assessment. Samples from the frontal, parietal, and occipital subcortical white matter, and spinal cord were stained according to Kluver-Barrera for myelin detection.

IHC staining was performed as reported previously (11). Supplementary Data Table S2 provides a list of primary antibodies that were used in a selected set of anatomical locations (Supplementary Data Table S3). Anti-CD68 staining was performed in all FFPE tissue blocks from the brain and spinal cord. Cerebellar cortex, brainstem nuclei of the floor of the fourth ventricle, and spinal anterior horns were processed for electron microscopy (12).

Histology and IHC slides were analyzed and imaged using Nikon Eclipse E800 microscope (Nikon, Tokyo, Japan) equipped with Olympus DP70 digital camera and DPControl software (Olympus, Tokyo, Japan). JEOL 1400+ transmission electron microscope (JEOL, Akishima, Tokyo, Japan) with Olympus Veleta CCD camera and Radius software (both Olympus) were used for ultrastructural analyses and imaging.

Long-Read Sequencing of the *NOTCH2NLC*-Specific PCR Products Containing the CGG Repeat

Genomic DNA from the patient's and healthy control's peripheral venous blood was isolated using the Gentra Pure-gene Blood Kit (Qiagen, Hilden, Germany) according to the manufacturer's protocol. To avoid nonspecific amplification of homologous genes (*NOTCH2NLA*, *NOTCH2NLB*, *NOTCH2NLR*, and *NOTCH2*) PCR primers (*NOTCH2NLC*_F—5'GATCGAGTTAAGGCTGCTGGA and *NOTCH2NLC*_R—5'CACCTTTC AAAGACGCGAGC) were designed to specifically amplify the CGG repeat-containing region of the *NOTCH2NLC* gene. LA Taq with GC buffer I (TaKaRa, Kyoto, Japan) and a two-step PCR protocol were used: Initial denaturation at 94°C for 5 minutes was followed by 24 cycles of 94°C for 15 seconds and 64°C for 4 minutes, final elongation was at 72°C for 10 minutes. The products (~1200 bp long) were purified using Agencourt AMPure XP magnetic beads (Beckman Coulter, Brea, CA) according to the manufacturer's protocol and sequenced on Pacific Biosciences Sequel system (PacBio, Menlo Park, CA).

To obtain highly accurate reads, Circular Consensus Sequence (CCS) analysis was performed using SMRT Link (v6.0). The number of repeats was determined directly from CCS reads. To confirm the results, CCS reads were aligned to *NOTCH2NLC* reference sequence (GRCh38) using bwa mem (version 0.7.17-r1188) and visualized in Integrative Genomics Viewer (2.3) (13).

Genomic sequence of *NOTCH2NLC* and sequences of the homologous genes *NOTCH2NLA*, *NOTCH2NLB*, *NOTCH2NLR*, and *NOTCH2* (GRCh38) were retrieved from the sequence database provided by the National Center for Biotechnology Information (NCBI) and their multiple sequence alignment was performed using Clustal Omega (1.2.4) (14).

Analysis of CGG Repeats in the 5' Untranslated Region of the *FMRI* Gene

Part of the *FMRI* 5' region that contained the CGG repeats expanded in Fragile X syndrome (FXS, MIM #300624) was PCR amplified using a pair of specific primers (FRAXA-R—5'AGCCCCGCACTTCCACCACCAGCTCCTCCA and FRAXA-F—5'GCTCAGCTCCGTTTCGGTTTCACTTCCGGT).

RESULTS

Case Report

The male patient was the second child of nonconsanguineous Caucasian parents. His older sister is healthy. The family has no history of hereditary genetic disease. The patient was born at term, spontaneously, and adapted normally. The patient's verbal development was delayed at 2 years, as he only used syllables at that age. Otherwise his psychosocial and motor development was normal.

The patient developed an intention tremor, an unsteady gait and a convergent strabismus at the age of 2 years and

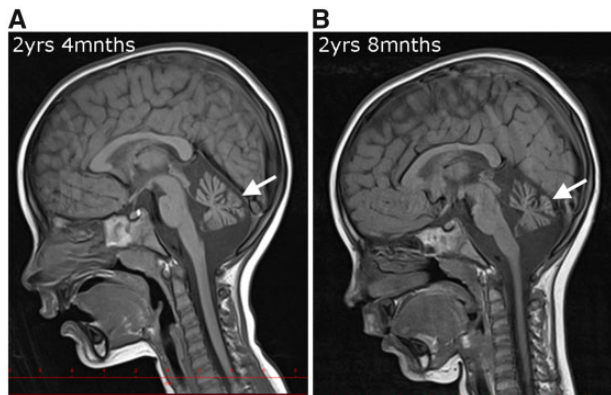


FIGURE 1. Brain MRI. Brain MRIs show progressive cerebellar atrophy (white arrows) in the patient at **(A)** 2 years and 4 months; **(B)** 2 years and 8 months.

4 months. Magnetic resonance imaging (MRI) showed cerebellar atrophy (Fig. 1A). Cerebrospinal fluid analyses were normal and did not suggest infectious or immune origin of the patient's clinical disease. Electromyography findings were normal. Electroencephalography (EEG) showed slower basal activity, however, no epileptic activity was identified.

Cerebellar ataxia rapidly worsened and at the age of 2 years and 8 months, the patient had a wide base gait and needed support while walking. Truncal ataxia, dysmetria, and dyssynergia appeared. Sleep EEG showed bilateral epileptiform discharges, however, symptomatic seizures were not observed. Cerebellar atrophy progressed on MRI (Fig. 1B). The patient was biochemically screened for metabolic diseases without any positive results. Skin biopsy samples were collected and evaluated by electron microscopy without any abnormality.

The patient's neurological functions deteriorated in the following years. His end-stage disease was categorized as a severe progressive neurodegenerative condition combining cerebellar, psychosocial and cognitive regression, pseudobulbar syndrome, and diminished deep tendon reflexes and muscle hypotonia in both upper and lower extremities due to mixed axonal and demyelinating polyneuropathy. The patient died at the age of 7 years due to chronic respiratory failure that was terminally exacerbated by bronchopneumonia.

Brain and Spinal Cord Pathology

Gross Pathology

At autopsy, the patient's brain weighed 1220 g (normal weight at 7 years of age is 1260 g). It was symmetrical and globation and gyrification were normal. Cerebellar hemispheres and cerebellar vermis were markedly atrophic. Cisterna magna (cerebellomedullary cistern) was dilated. Spinal cord was without any obvious abnormality. Atrophy of ventral or dorsal roots was not evident.

Histology and Immunohistochemistry

Neuronal eosinophilic hyaline intranuclear inclusions were the most prominent abnormality identified in all tissue samples from the brain and spinal cord (Fig. 2). The majority of nuclei contained a single inclusion. On occasion, nuclei contained multiple or "snowman-like" inclusions. The inclusions stained positive with anti-ubiquitin and anti-p62 antibodies and were observed almost exclusively in neurons (Fig. 2). Kluver-Barrera staining did not suggest prominent white matter myelin changes in any of the cerebral or spinal cord areas.

CD68-positive microglia/macrophages were numerous and had an activated morphology in gray and white matter areas of all sampled neuroanatomic locations (Fig. 3A–F). CD68-positive clusters suggested extensive neuronophagy and were widely distributed in the brain. Cortical layer V (of nearly all cortical areas tested) and CA3 and CA4 parts of hippocampus were particularly affected by neuronophagy (Fig. 3B–D). Local axonophagy was observed in cerebral white matter (Fig. 3E).

Histology sections from all parts of the spinal cord showed dilated ventral median fissure. CD68-positive cellular clusters were not frequent or prevalent in any part of the spinal gray matter though CD68-positive cells were numerous in spinal white matter tracts. Fasciculus gracilis was the area most affected by axonophagy (Fig. 3F).

The cerebellar cortex was substantially thinned. Numeric atrophy was found in molecular, Purkinje cells and granular layers. Excessive astrogliosis was identified by anti-GFAP IHC staining. Compared with the majority of cerebral locations, the population of CD68-positive microglia/macrophages was relatively sparse and mostly limited to perivascular areas (Fig. 4A). Neuronophagic clusters were not found in cerebellum as a likely reflection of the already burnt-out degenerative pathology (Fig. 4B). Residual Purkinje cells were with intranuclear inclusions (Fig. 4C). Cerebellar white matter was also substantially reduced.

Electron Microscopy

The neuronal intranuclear inclusions appeared similar in all anatomic regions analyzed. They had a fibrillary "criss-crossed wool-like" appearance and lacked a limiting membrane (Fig. 4D). Some inclusions had a denser core.

Skin Biopsy: Histopathology, Immunohistochemistry, and Electron Microscopy

Skin biopsy was collected from the patient at the age of 2 years and 8 months and no abnormality was identified by histological and ultrastructural analyses. The sample was re-evaluated after the diagnosis of iNIID was set by postmortem neuropathology evaluation (7 years of age). Similar to the previous findings, no abnormalities were identified and intranuclear inclusions could not be detected by anti-p62 or anti-ubiquitin IHC and electron microscopy.

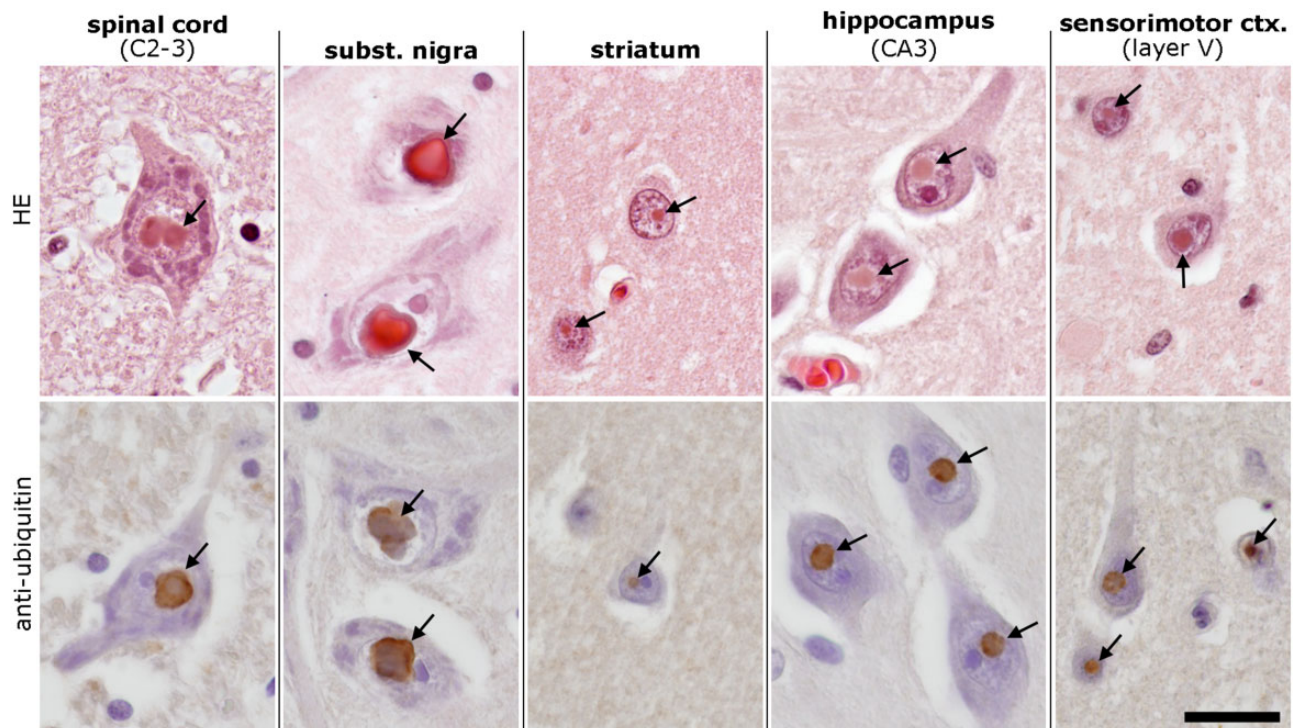


FIGURE 2. Neuronal intranuclear inclusions are detectable by the hematoxylin and eosin stain and anti-ubiquitin immunohistochemistry. Upper row of images: eosinophilic hyaline intranuclear inclusions (black arrows) in various neuronal populations. Inclusions stain (black arrows in the lower row of images) with anti-ubiquitin primary antibody. Scale bar = 20 μ m.

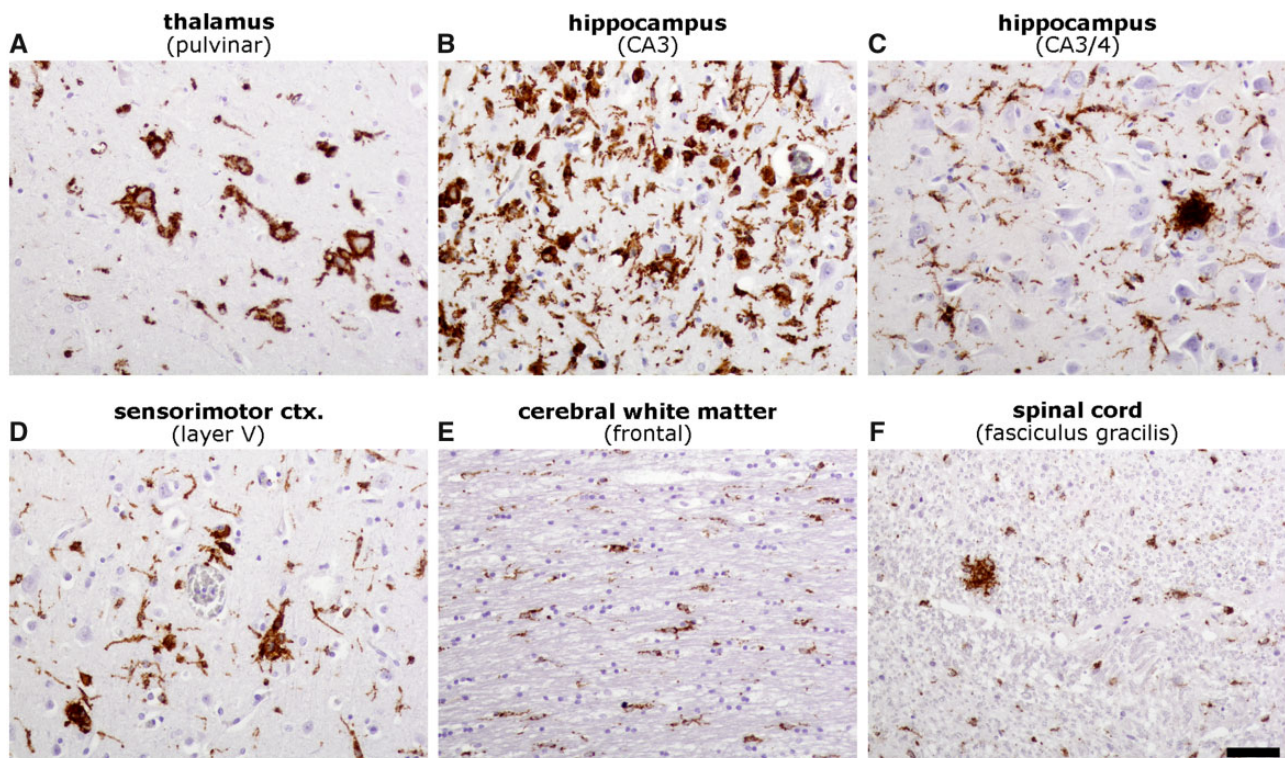


FIGURE 3. Microglia/macrophage abnormalities: anti-CD68 immunohistochemistry. **(A–D)** CD68⁺ neuronophagic clusters in a broad array of gray matter locations. **(E, F)** CD68⁺ microglia/macrophages are numerous in cerebral and spinal white matter. Axonophagy was detected particularly in the spinal cord. Scale bar = 50 μ m.

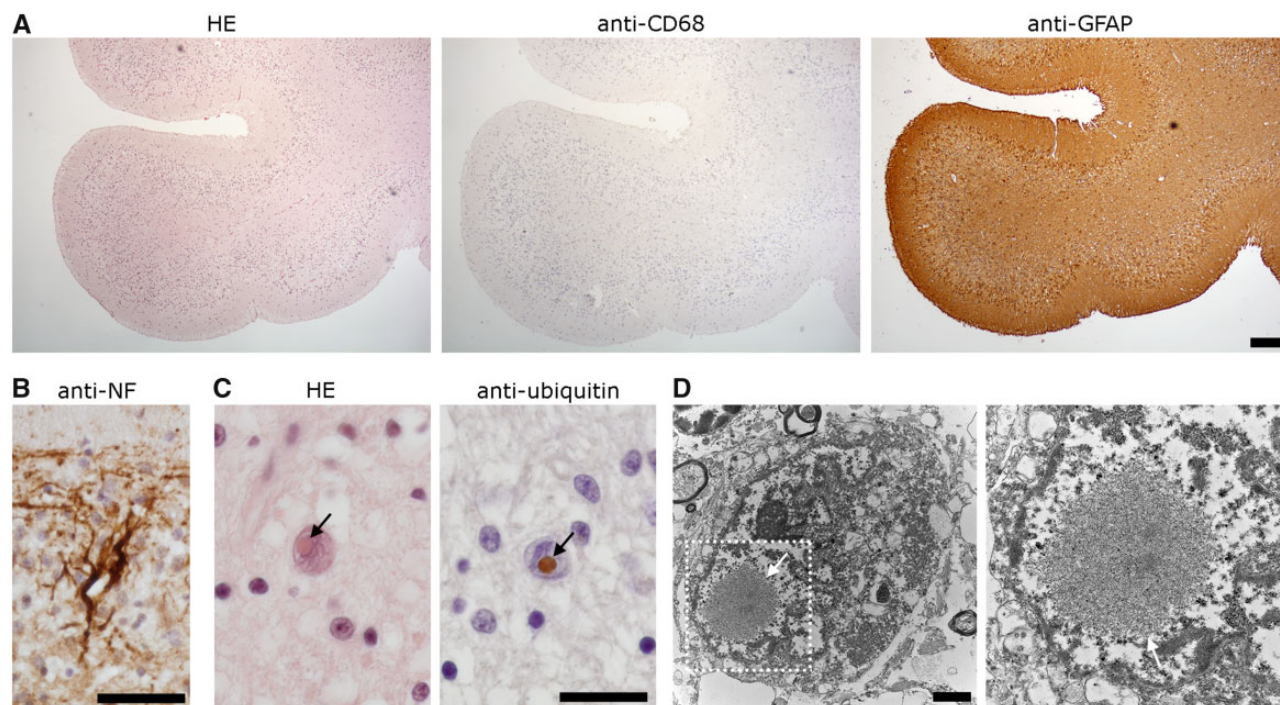


FIGURE 4. Cerebellar atrophy. **(A)** All 3 cerebellar cortical layers (molecular, Purkinje cells [PC], and granule cells) are reduced. Cerebellar white matter is also atrophic. Population of CD68+ microglia/macrophages is sparse. GFAP+ astrogliosis is extensive. **(B)** “Empty” PC basket highlighted by IHC staining with anti-neurofilament (NF) primary antibody. **(C)** Intranuclear inclusions in residual PCs stain positive with anti-ubiquitin antibody (black arrows). **(D)** Intranuclear inclusions (shown in a single PC) have the typical “criss-crossed” appearance by electron microscopy. To demonstrate the absence of the limiting membrane, the inclusion highlighted by the white arrow and dotted square is shown at a higher magnification. Scale bars: **A** = 200 μ m, **B**, **C** = 20 μ m, **D** = 2 μ m.

Visceral Organs—Histopathology and Immunohistochemistry

Intranuclear inclusions could not be reliably identified by histological stains or IHC (anti-p62 and anti-ubiquitin) in any of the visceral organs evaluated. Alveolar septa were congested and acute suppurative bronchopneumonia (locally forming microabscesses) was identified in both lungs. Kidneys had a congested corticomedullary junction. Sporadic microabscesses were found in cortical tubules. Spleen and liver were congested. Myocardium had no major abnormalities. Some cardiomyocytes had enlarged nuclei suggesting very mild hypertrophy.

NOTCH2NLC CGG Repeat Analyses

We performed long-read sequencing of the *NOTCH2NLC* PCR amplicon that contained the critical repeat motif (Fig. 5A) and found it in a heterozygous allelic setup: $AGG(CGG)_9(AGG)_2CGG/AGG(CGG)_{15}(AGG)_2CGG$ (Fig. 5B). The number (9 and 15) of CGG repeats in the patient’s genomic DNA corresponded to values identified in healthy individuals as reported by others (7–10).

FMR1 CGG Repeats Analyses

Neuronal intranuclear inclusions were reported in patients with fragile X-associated tremor/ataxia syndrome (15,

16). CGG triplets in the 5’ untranslated region of the *FMR1* gene were not expanded in the iNIID patient (Supplementary Data Fig. S1).

DISCUSSION

In this report, we present a 7-year-old patient with a severe progressive neurodegenerative disease that included cerebellar symptoms with cerebellar atrophy, psychomotor developmental regression, pseudobulbar syndrome, and polyneuropathy. Postmortem tissue analyses identified iNIID in the patient. Characteristic neuronal intranuclear inclusions with the typical IHC profile were found in the patient’s nervous system. Skin biopsy, which was collected and analyzed antemortem at the age of 2 years and 8 months and was re-evaluated after the patient’s death, did not show intranuclear inclusions.

We commend the authors of the 4 aforementioned studies (7–10) for identifying the *NOTCH2NLC* CGG expansions in their cohorts of adult (and juvenile) NIID patients. To the best of our knowledge, the patient presented in this manuscript is the first iNIID patient who was tested for the number of *NOTCH2NLC* CGG repeats. In reference to findings by Ishiura et al in the adult patients, the absence of the *NOTCH2NLC* CGG expansions in our patient provides additional evidence suggesting genetic heterogeneity of NIID (8). The documented patient is also the second one who lacked skin biopsy

13. Robinson JT, Thorvaldsdottir H, Wenger AM, et al. Variant review with the integrative genomics viewer. *Cancer Res* 2017;77:e31–e4
14. Madeira F, Park YM, Lee J, et al. The EMBL-EBI search and sequence analysis tools APIs in 2019. *Nucleic Acids Res* 2019;47:W636–W41
15. Wheeler A, Raspa M, Hagerman R, et al. Implications of the FMR1 pre-mutation for children, adolescents, adults, and their families. *Pediatrics* 2017;139:S172–S82
16. Gelpi E, Botta-Orfila T, Bodi L, et al. Neuronal intranuclear (hyaline) inclusion disease and fragile X-associated tremor/ataxia syndrome: A morphological and molecular dilemma. *Brain* 2017;140:e51

LETTER

Genetic heterogeneity of neuronal intranuclear inclusion disease: What about the infantile variant?

Jakub Sikora^{1,2} , Ivana Jedlickova¹, Anna Pristoupilova¹, Viktor Stranecky¹ & Tomas Honzik¹

¹Research Unit for Rare Diseases, Department of Paediatrics and Inherited Metabolic Disorders, First Faculty of Medicine, Charles University and General University Hospital, Prague, Czech Republic

²Institute of Pathology, First Faculty of Medicine, Charles University and General University Hospital, Prague, Czech Republic

Correspondence

Jakub Sikora, Research Unit for Rare Diseases, Department of Paediatrics and Inherited Metabolic Disorders, First Faculty of Medicine, Charles University and General University Hospital, Prague, Czech Republic, Ke Karlovu 2, 128 00 Prague 2, Czech Republic. Tel: +420 224 967 041; Fax: +420 224 911 453; Email: jakub.sikora@lf1.cuni.cz

Funding Information

Ministerstvo Zdravotnictví České Republiky: NV19-08-00137

Received: 25 November 2020; Accepted: 28 January 2021

Annals of Clinical and Translational Neurology 2021; 8(4): 994–1001

doi: 10.1002/acn3.51332

Dear Editor,

Chen et al.¹ have demonstrated lack of abnormal CGG expansions in the *NOTCH2NLC* gene among European juvenile and adult patients with neuronal intranuclear inclusion disease (jNIID and aNIID). Genetic heterogeneity of NIID was suggested based on the discrepancy of these results and earlier findings in East Asian patients.^{2–5}

We recently studied⁶ *NOTCH2NLC* CGG repeats in an infantile NIID (iNIID) patient independently of Chen et al.¹ This Caucasian European boy is the first, and thus far only, iNIID patient who has been tested for this molecular pathology. The number of repeats in this patient corresponded to values found in healthy controls. We believe that these data provide further evidence^{1,3} for genetic heterogeneity of NIID. It is, however, important to highlight that our results do not, at this point, allow conclusions about genetic causes of NIID among European patients of all age groups or about genetic causes of iNIID.

We recognize the diagnostic criteria for NIID-related diseases that were suggested by Chen et al.¹ However, it is our impression that their algorithm/flowchart considers juvenile and adult NIID patients but the distinctive characteristics of iNIID have not been sufficiently reflected. To help the diagnostic practice, we provide a summary of clinical (Table 1) and (neuro)pathological (Table 2) findings in iNIID patients.

iNIID is a rare and rapidly progressive neurodegenerative pediatric disease.^{7,8} To the best of our knowledge, there have been eight ethnically diverse iNIID patients

reported.^{6,8–14} All were diagnosed by *post-mortem* neuropathology work-up. Seven patients developed the first symptoms prior to or by 5 years of age and died before reaching 10 years of age. Only one patient presented and died older.⁹

The following developmental and clinical characteristics are key phenotypic features of iNIID: (i) early development is more-or-less normal, the onset of disease is abrupt and the progression is rapid; (ii) initial symptoms almost always involve unsteady gait and/or movement abnormalities associated with cerebellar dysfunction, (iii) the terminal neurological disease is associated with cerebellar decline, progressive pseudobulbar or bulbar palsy, peripheral neuropathy, hypotonia, and severe psychosocial regress, and (iv) respiratory infection or respiratory failure-associated pathologies are the most common causes of death. Major non-neurological abnormalities were reported in only one iNIID patient, who suffered from dilated cardiomyopathy and developed congestive heart failure.¹³

Neuroimaging frequently identifies early-onset cerebellar atrophy in iNIID. Contrary to aNIID,¹⁵ there is no information about CNS corticomedullary junction abnormalities and the diagnostic utility of diffusion-weighted MRI in iNIID patients is unknown.

Intranuclear inclusions (IIs) were not found in *ante-mortem* skin biopsies of three iNIID patients.^{6,9,10} Skin biopsy of the fourth iNIID patient was reported as normal (presence or absence of IIs was not explicitly noted).¹¹

Neuronal IIs are widespread in the central (and also peripheral) nervous system in iNIID patients. IIs in non-neuronal CNS cell types have been unambiguously

Table 1. Clinical history of previously published iNIID patients.

	Sex // ethnicity-nationality // family history	Pre- and perinatal history // early development	Disease onset // initial symptoms	Disease progression	Age at death // cause of death	Brain imaging // electrophysiology
Patel et al. (1985)	F // North American Indian// unaffected nonconsanguineous parents	born 1 mth premature (2.2 kg) // developed normal, but free walked at 1.5 yrs; speech delay; poor articulation	3.5 yrs // unsteady gait (frequent falls), hypotonia, areflexia, scoliosis, delayed behavioral development, microcephaly (−2SD)	seizures, ataxia, nystagmus, choreoathetosis, cranial nerve palsies, extensor plantar reflexes, poor strength and tone in the arms, sensory deficits in the extremities, diminished pupillary reactions, elevated blood pressure, attacks of bradycardia, and tachycardia 6.5 yrs - developmentally delayed to 4mths	6 yrs 10mths // bronchopneumonia, emaciated at autopsy	CT (age <i>n.r.</i>) - large ventricles, sulci and cisterns // mild sensory neuropathy (3.5 yrs) severe mixed peripheral neuropathy (6.5 yrs) EEG (age <i>n.r.</i>) - diffuse and later bursts of slow activity ECG (age <i>n.r.</i>) - normal
Garen et al. (1986)	M // <i>n.r.</i> // no family history of neurological diseases	uncomplicated pregnancy and delivery // neurologically normal until 5 yrs	5 yrs // episodes of loss of motor control in lower extremities (unable to walk), ataxia, transient choreoathetosis	6-7 yrs - increased frequency of motor control loss, progression of dyskinesia, IQ 91 8 yrs - impaired tandem walking, dysmetria, dysarthria, dysphagia, incontinence, blepharospasm 9 yrs - intention myoclonus, conjugate deviation of eyes, episodic nystagmus, cognitive regression, marked tremor and rigidity in the arms, hypotonia of legs, areflexia, immobile, unable to chew or swallow, gastrostomy	9.5 yrs // pneumonia	CT (9 yrs) – unspecified mild atrophic changes // VEPs and BAERs (age <i>n.r.</i>) - mildly abnormal slow conduction in peroneal nerves (age <i>n.r.</i>) EEG (9 yrs) - slow waves
Oyer et al. (1991)	M // white // <i>n.r.</i>	born premature (36wks) // normal development until 3 yrs	3 yrs // incoordination and disturbed gait	3-6 yrs - loss of speech and head control, ptosis, athetosis, drooling 8 yrs - congestive heart failure and pneumonia	9 yrs // <i>n.r.</i>	MRI (6 yrs) - atrophy of cerebral cortex, cerebellum, cerebral peduncles, and olives

(Continued)

Table 1. Continued.

	Sex // ethnicity-nationality // family history	Pre- and perinatal history // early development	Disease onset // initial symptoms	Disease progression	Age at death // cause of death	Brain imaging // electrophysiology
Sloane et al. (1994)	M // n.r. // healthy nonconsanguineous parents and older brother, maternal uncle and grandmother – Parkinson disease, maternal first cousin – intellectual disability of unknown cause	uncomplicated pregnancy and delivery, born at term (3460 g) // motor development normal until 3 yrs	2.5 yrs // ataxia, speech delay, seizures	3 yrs 1 mth - delay in all areas of Yale Developmental Schedule 3.5 yrs - progressive ataxia (wheelchair bound), resting tremor, titubation, incontinence, speech deterioration, loss of communication skills, myoclonic and absence seizures refractory to therapy 4.5 yrs - little verbal and non-verbal communication, nystagmus, bilateral internuclear ophthalmoplegia, generalized hypotonia, mild pes cavus, marked truncal and appendicular ataxia	4 yrs 4 mths // found unconscious at home, acute bronchitis and pulmonary edema at autopsy	CT (3.5 yrs) - cerebellar atrophy MRI (consequent to CT) - vestigial vermis and superior vermal atrophy, small brainstem, dilated aqueduct, 4th ventricle and CSF spaces // EEG (2.5 yrs) - generalized spike-and-wave activity, later generalized slow waves BAERs (age n.r.) - hearing loss, poor delineation of wave 1 but normal central conduction VERs, somatosensory EPs in median nerve, and peripheral motor nerve conduction (age n.r. in all) - normal.
McFadden (2005)	M // n.r. // no family history of dementia, developmental or movement disorders, motor handicaps or seizures	uncomplicated pregnancy and delivery // normal early developmental milestones	7.5 yrs // tremors of hands, difficulty walking, required assistance after falling, leg pain and weakness, stiff-legged	8 yrs - action and sustension tremor, bilateral weakness of lower legs, decreased deep tendon reflexes, pes planus, impaired speech articulation	13 yrs // respiratory infection and failure, emaciated and with generalized muscle atrophy at autopsy	MRI (8 yrs + 9.5 yrs) - mild enlargement of cerebellar sulci and mild vermian atrophy // reduced motor and sensory conduction velocities in both upper

(Continued)

Table 1. Continued.

Sex // ethnicity-nationality // family history	Pre- and perinatal history // early development	Disease onset // initial symptoms	Disease progression	Age at death // cause of death	Brain imaging // electrophysiology
		gait, right leg rotated outwards	9 yrs - wheelchair bound, no speech, difficulty swallowing, excessive drooling, coarse tremor with episodes of whole body shaking, positive extensor plantar reflexes, oculogyric crises 11 yrs - constant tremor of hands, unable to hold head erect, drooling (atrophic tongue with fasciculations), generalized muscular atrophy, contractures and areflexia		and lower extremities (8 yrs) sural sensory action potential (8 yrs) - unobtainable electromyography (8 yrs) - denervation/ reinnervation changes without evidence of recent denervation ECG (8 yrs) - normal
M // Japanese // no family history of neurological illnesses	normal pregnancy and delivery, born at 40 wks (2520 g), neonatal period uneventful // psychomotor development normal until 2 yrs	2 yrs // afraid of walking	4 yrs - progressive deterioration, open mouth, hypersalivation, generalized hypotonia, spasticity in lower limbs with hyperactive deep tendon reflexes, slurred speech, ataxia, unable to stand or walk without support 5-7 yrs - worsened bulbar palsy, unable to sit unsupported, seldom speaking, dysphagia, intellectual deterioration, gavage feeding, tracheostomy, bedridden	7 yrs // respiratory failure, hypoventilation, pneumonia	MRI (2 yrs) - marked cerebellar atrophy; MRI (4 yrs) - severe atrophy of vermis and cerebellar hemispheres, mild brainstem atrophy, no cerebellar atrophy, no myelination abnormality; SPECT (4 yrs) - cerebellar hypoperfusion; MRI (5-7 yrs) - severe cerebellar and cerebral (grey and also little in white matter) atrophy // EEG (4 yrs) slow basic rhythm, no paroxysmal activity; normal peripheral nerve conductance (4 yrs),

(Continued)

Table 1. Continued.

Sex // ethnicity-nationality // family history	Pre- and perinatal history // early development	Disease onset // initial symptoms	Disease progression	Age at death // cause of death	Brain imaging // electrophysiology
F // African // <i>n.r.</i>	<i>n.r.</i> // appeared to develop normally until 4 yrs	4 yrs // found convulsing and febrile, seizures since then, dyskinesia, unable to walk or sit unsupported	5.5 yrs – developmental regression, increased seizure activity, poor central tone, reduced global power, loss of pincer grasp, limited vocabulary, nystagmus	6.5 yrs // aspiration pneumonia, upper and lower limb wasting at autopsy	MRI (5.5 yrs) - dilatation of the 4th ventricle, significant cerebellar atrophy
M // Caucasian-Czech // no family history of neurological illnesses, healthy parents and older sister	born at term, spontaneously adapted normally // psychosocial and motor development normal until 2 yrs, verbal development delayed at 2 yrs	2 yrs 4 mths // intention tremor, ataxia, convergent strabismus	2 yrs 8 mths – rapidly progressive cerebellar ataxia terminal neurologic disease - severe progressive neurodegenerative condition with psychosocial and cognitive regression, pseudobulbar syndrome, mixed axonal and demyelinating polynuropathy	7 yrs // chronic respiratory failure with terminal bronchopneumonia	MRI (2 yrs 4 mths) - cerebellar atrophy MRI (2 yrs 8 mths) - progressed cerebellar atrophy // EEG (2 yrs 4 mths) - slower basal activity, no epileptic activity sleep EEG (2 yrs 8 mths) - bilateral epileptiform discharges (no symptomatic seizures)

Abbreviations: BAERs, brain stem auditory-evoked responses; CT, computer tomography; ECG, electrocardiography; EEG, electroencephalography; EP, evoked potentials; F - female; M, male; MRI, magnetic resonance imaging; mths, months; *n.r.*, not reported; SD, standard deviation; SPECT, single-photon emission CT; VERs, visual-evoked responses; wks, weeks; yrs, years.

Table 2. Biopsy and autopsy findings in iNIID patients.

	Ante-mortem biopsies	Brain weight (g) // gross CNS pathology	CNS histopathology	Ultrastructure of the intranuclear inclusions	Pathology of non-CNS tissues
Patel et al. (1985)	skin bs (age n.r.) - normal skeletal muscle bs (age n.r.) - normal peripheral (sural) nerve bs (age n.r.) - increased endoneural collagen and some loss of unmyelinated axons	900 // mild frontal gyral atrophy, slightly enlarged left lateral ventricle, small semioval center, cerebellar vermal atrophy	widespread neuronal IIs neurodegeneration - PCs, granule cells layer neurons, thalamus, DN mild myelin loss in the mid-portions of the posterior (spinal) columns in the mid-thoracic area and caudad	ranging from grey fluffy masses to filamentous	DRG neurons, autonomic ggl., myenteric plexi neurons - IIs mild myelin pallor of the lumbal dorsal roots cells of the adrenal medulla and anterior pituitary gland - IIs
Garen et al. (1986)	n.r.	1160 // no atrophy of the brain; gray and white matter grossly normal; pale SN; no atrophy of SC	widespread IIs confined to neurons neurodegeneration - pigmented SN neurons, Clarke's column neurons, PCs with hypoxic/ischemic alterations mild loss of myelin in fasciculus gracilis, ventral and dorsal spinocerebellar tracts	filamentous with dense core (some granularity at high magnification)	DRG neurons - IIs
Oyer et al. (1991)	n.r.	1119 // olivary bulges slightly atrophic; subthalamic nuclei difficult to distinguish; firm pyramidal tracts and olivary nuclei; atrophy of the cerebellar folia	widespread neuronal IIs	granular (in cardiomyocytes)	DRG neurons - IIs dilated cardiomyopathy with fibrosis (heart weight - 273g) cardiomyocytes - IIs skeletal muscle with atrophy but no IIs
Sloane et al. (1994)	n.r.	590 // normal cerebral hemispheres, brain stem and spinal cord; small cerebellum with atrophy of hemispheres and vermis; dilated 4th ventricle	widespread neuronal IIs; severe cerebellar ctx atrophy neurodegeneration - PCs, granule cells layer neurons, and DN	filamentous	DRG neurons, sympathetic ggl. and myenteric plexi neurons - IIs hepatocytes - IIs skeletal muscle (deltoid and quadriceps) - no abnormality
McFadden (2005)	sural nerve bs (8 yrs) - axonal degeneration and regeneration skin biopsy (8 yrs) - no IIs in any cell type	1425 // atrophy of the cerebellar hemisphere and vermis (hemidivided brain), mild atrophy of the SC ventral roots	widespread neuronal IIs, glial IIs not seen neurodegeneration - subthalamic nucleus, SN, red ncl., cerebellar ctx (severe PC loss, moderate granular cells loss), DN, SC anterior horn cells IHC - IIs SUMO-1+, ubiquitin+, glucocorticoid receptor+ deep white matter well myelinated	randomly oriented filaments and electron-dense granular material	neurons of the adrenal medulla and Auerbach's plexus - IIs cardiac cells - occasional IIs

(Continued)

Table 2. Continued.

	Ante-mortem biopsies	Brain weight (g) // gross CNS pathology	CNS histopathology	Ultrastructure of the intranuclear inclusions	Pathology of non-CNS tissues
Mano et al. (2007)	superficial rectal bs - not conclusive	1080 // cerebellar and brainstem atrophy	widespread neuronal IIs, <5% of astrocytes with IIs, oligodendrocytes, ependymal and endothelial cells with no IIs marked neurodegeneration of the cerebellar ctx and inferior olive, moderate to mild neurodegeneration in DN and pontine nuclei, mild degeneration in cerebral ctx, striatum and ventral SC horns myelin pallor due axonal loss in the cerebral hemisphere, cerebral peduncles, medullary pyramid and SC corticospinal tract IHC - IIs ubiquitin+	microfibrillary	DRG - IIs, Meissner and Auerbach plexus - occasional IIs
Pilson et al. (2017)	skin bs (collected 7mths prior death) - no IIs reported muscle bs (age <i>n.r.</i>) - neurogenic atrophy	<i>n.r.</i> // normal cortical mantle, atrophic cerebellar vermis, dilated 4th ventricle	widespread neuronal IIs cerebellar atrophy with PC loss and Bergmann gliosis IHC - IIs p62+, ubiquitin+	<i>n.r.</i>	myenteric plexus of the esophagus, stomach, appendix, and small and large intestines, parasympathetic ganglia and neural crest cells of the adrenal medulla - IIs
Jedlickova et al. (2020)	skin bs (2 yrs 8 mths) - no IIs	1220 // normal cerebral globation and gyrrification, atrophy of cerebellar vermis and hemispheres	widespread and almost exclusively neuronal IIs widespread neurodegeneration, severe cerebellar atrophy with PC loss and astrocytosis IHC - IIs p62+, ubiquitin+	fibrillary	lungs, spleen, kidneys, liver and myocardium - no IIs

Abbreviations: bs, biopsy; CNS, central nervous system; ctx, cortex; DN, dentate nucleus; DRG, dorsal root ganglia; ggl, ganglia; IHC, immunohistochemistry; IIs, intranuclear inclusions; mths, months; *n.r.*, not reported; ncl, nucleus; PCs, Purkinje cells; SC, spinal cord; SN, substantia nigra; yrs, years.

reported in only one patient (less than 5% of astrocytes contained IIs).⁸ The extent and distribution of CNS neuronal loss may be variable, however, cerebellar (cortical) atrophy is almost universally present in iNIID patients. Mild myelin loss and/or pallor in different CNS regions was noted only occasionally.

To summarize: iNIID is a severe early childhood-onset neuropediatric disease. Some of the key clinical, neuroimaging and (neuro)pathology characteristics that allow *ante-mortem* identification of jNIID and aNIID may not be useful to diagnose iNIID patients. Understanding the genetic background of iNIID is a critical component to allow effective diagnostics, counselling and future therapy development. With this information at hand, we are prepared to collaboratively study our data with samples from other children with iNIID or within cohorts of juvenile and adult NIID individuals.

Acknowledgments

This work was supported by the research grant (NV19-08-00137) from the Ministry of Health of the Czech Republic.

Conflict of Interest

All authors report no disclosures.

References

- Chen Z, Yan Yau W, Jaunmuktane Z, et al. Neuronal intranuclear inclusion disease is genetically heterogeneous. *Ann Clin Transl Neurol.* 2020;7(9):1716–1725.
- Sone J, Mitsuhashi S, Fujita A, et al. Long-read sequencing identifies GGC repeat expansions in NOTCH2NLC associated with neuronal intranuclear inclusion disease. *Nat Genet.* 2019;51(8):1215–1221.
- Ishiura H, Shibata S, Yoshimura J, et al. Noncoding CGG repeat expansions in neuronal intranuclear inclusion disease, oculopharyngodistal myopathy and an overlapping disease. *Nat Genet.* 2019;51(8):1222–1232.
- Tian Y, Wang JL, Huang W, et al. Expansion of human-specific GGC repeat in neuronal intranuclear inclusion disease-related disorders. *Am J Hum Genet.* 2019;105(1):166–176.
- Deng J, Gu M, Miao Y, et al. Long-read sequencing identified repeat expansions in the 5'UTR of the NOTCH2NLC gene from Chinese patients with neuronal intranuclear inclusion disease. *J Med Genet.* 2019;56(11):758–764.
- Jedlickova I, Pristoupilova A, Hulkova H, et al. NOTCH2NLC CGG repeats are not expanded and skin biopsy was negative in an infantile patient with neuronal intranuclear inclusion disease. *J Neuropathol Exp Neurol.* 2020;79(10):1065–1071.
- Takahashi-Fujigasaki J. Neuronal intranuclear hyaline inclusion disease. *Neuropathology.* 2003;23(4):351–359.
- Mano T, Takizawa S, Mohri I, et al. Neuronal intranuclear hyaline inclusion disease with rapidly progressive neurological symptoms. *J Child Neurol.* 2007;22(1):60–66.
- McFadden K, Hamilton RL, Insalaco SJ, et al. Neuronal intranuclear inclusion disease without polyglutamine inclusions in a child. *J Neuropathol Exp Neurol.* 2005;64(6):545–552.
- Pilson K, Farrell M, Lynch B, Devaney D. A case of juvenile onset neuronal intranuclear inclusion disease with a negative antemortem skin biopsy. *Pediatr Dev Pathol.* 2018;21(5):494–496.
- Patel H, Norman MG, Perry TL, Berry KE. Multiple system atrophy with neuronal intranuclear hyaline inclusions. Report of a case and review of the literature. *J Neurol Sci.* 1985;67(1):57–65.
- Sloane AE, Becker LE, Ang LC, Wark J, Haslam RH. Neuronal intranuclear hyaline inclusion disease with progressive cerebellar ataxia. *Pediatr Neurol.* 1994;10(1):61–66.
- Oyer CE, Cortez S, O'Shea P, Popovic M. Cardiomyopathy and myocyte intranuclear inclusions in neuronal intranuclear inclusion disease: a case report. *Hum Pathol.* 1991;22(7):722–724.
- Garen PD, Powers JM, Young GF, Lee V. Neuronal intranuclear hyaline inclusion disease in a nine year old. *Acta Neuropathol.* 1986;70(3–4):327–332.
- Sone J, Mori K, Inagaki T, et al. Clinicopathological features of adult-onset neuronal intranuclear inclusion disease. *Brain.* 2016;139(Pt 12):3170–3186.